J. Fluid Mech. (2005), *vol.* 541, *pp.* 317–344.
doi:10.1017/S0022112005006142 Printed in the United Kingdom

Analytical and numerical studies of the stability of thin-film rimming flow subject to surface shear

By M. VILLEGAS-DÍAZ[1], H. POWER[1] AND D. S. RILEY[2]

[1]School of Mechanical, Manufacturing and Engineering Management, University of Nottingham, University Park, Nottingham NG7 2RD, UK

[2]Division of Applied Mathematics, School of Mathematical Sciences, University of Nottingham, University Park, Nottingham NG7 2RD, UK
david.riley@nottingham.ac.uk

(Received 28 July 2004 and in revised form 11 February 2005)

Motivated by applications in rapidly rotating machinery, we have previously extended the lubrication model of the thin-film flow on the inside of a rotating circular cylinder to incorporate the effect of a constant shear applied to the free surface of the film and discovered a system rich in film profiles featuring shock structures. In this paper, we extend our model to include the effects of surface tension at leading order and take into account higher-order effects produced by gravity in order to resolve issues regarding existence, uniqueness and stability of such weak solutions to our lubrication model. We find, by analytical and numerical means, a set of feasible steady two-dimensional solutions that fit within a rational asymptotic framework. Having identified mathematically feasible solutions, we study their stability to infinitesimal two-dimensional disturbances. Based on our findings, we conjecture which of the possible weak solutions are physically meaningful.

1. Introduction

There is a substantial and growing literature on thin-film flows on the inside (rimming flow) or outside (coating flow) of a rotating circular cylinder. The earliest work, Ruschak and Scriven (1976) and Orr and Scriven (1978), was concerned with the case when the fluid is in almost rigid-body rotation and the effects of gravity are small. Subsequently, the focus has shifted away from this parameter regime, but the coating and rimming flows that develop on the high-speed shafts within a modern aeroengine bearing chamber are closer to Scriven's parameter values.

Motivated by such considerations, Noakes, King & Riley (2005) consider the linear stability of rigidly rotating circular films in the absence of gravity. They systematically examine three-dimensional disturbances under the assumptions that the liquid filling fraction is small and that there is a continuous film coating the surface of the cylinder. Both asymptotic and numerical results suggest that the most unstable mode for thin-film flows on the inside surface of a cylinder is purely axial (ring instability); the asymptotically determined critical wavenumber is shown to depend solely on the reciprocal Weber number S, which must be greater than unity for instability to occur. When the filling fraction takes moderate values, however, instability can occur when $S < 1$. Noakes *et al.* also identify the critical wavenumber with maximum growth rate for thin-film flows on the outside surface of a cylinder. For small reduced

Reynolds numbers and $S > 1$, the disturbance is purely axial (ring instability), but when $0 < S < 1$ the most unstable disturbance may be either a purely axial or a purely azimuthal mode. The numerical results, however, suggest that, as the mode with the highest growth rate, a stripe instability (azimuthal mode) is likely to occur. While agreeing with some experimental evidence, this result conflicts with results from other experiments, suggesting that effects ignored in their study, gravity for example, even though weak, can play a significant role in mode selection, see Noakes *et al.* (2005).

Revallo & Riley (2004) make considerable analytical progress in the case of rimming flow having asymptotically small mean film thickness by treating gravitational effects as weak and perturbing about the Scriven solution. Their systematic approach enables them to explore both the effects of strong applied surface shear and of weak inertia. Asymptotic expressions are derived for the base state, the modes of disturbance and their growth rates. Consistent with the results of Noakes *et al.* (2005), the most unstable mode is purely axial (ring instability) for moderate values of the surface tension. When surface tension is weak, the most unstable modes have low azimuthal and axial wavenumbers. Furthermore, the effects of surface tension and inertia are in competition, and the destabilizing effect of inertia may be totally mitigated depending on the size of the surface shear. It is worth remarking that one well-known example of a ring-type instability is the so-called hygrocyst, Balmer (1970). Thoroddsen & Mahadevan (1997) state that the combination of high filling fraction and large viscosity leads to the formation of these radial sheets of fluid that span the whole cross-section and partition the cylinder; furthermore, their experimental data reveals that they occur at higher rotation rates. The axial instability mentioned above could represent the birth of this feature as fluid accumulates to produce a locally high value of the filling fraction.

As mentioned above, the majority of studies have concentrated on the complementary situation when rotation rates are lower and the effects of gravity are order one, see Ashmore, Hosoi & Stone (2003) for a recent comprehensive review. Benjamin, Pritchard & Tavener (1993), building on a study by Johnson (1988), investigate how solutions to the basic lubrication model that feature shocks are smoothed by the incorporation of higher-order effects due to gravity and, in addition, to surface tension, an aspect later studied in more depth by Wilson & Williams (1997). Benjamin *et al.* prove smooth two-dimensional solutions to the lubrication-model equations (no surface tension) are neutrally stable to two-dimensional (azimuthal) modes of disturbance (they briefly discuss three-dimensional effects). They also demonstrate asymptotic stability of a supercritical weak solution with a shock in the lower quadrant on the rising side of the cylinder. Hosoi & Mahadevan (1999) show stability of two-dimensional flows to three-dimensional perturbations in the presence of surface tension. In addition to a linear instability analysis, Hosoi & Mahadevan conduct numerical studies by allowing time-dependent solutions to evolve to steady states. By solving at parameter values outside the range for which the equations are strictly valid, they capture fascinating shark-teeth patterns as observed experimentally by Johnson (1990) and by Thoroddsen & Mahadevan (1997). Hosoi & Mahadevan highlight that this pattern results when a spatially localized ridge (a region of rapid change in the profile height) is perturbed axially, and thicker regions travel faster than thinner ones. The destabilizing mechanism is due to gravitational and viscous forces, but wavelength selection is controlled by capillary and viscous forces.

O'Brien (2002*a*) confirms the results of Benjamin *et al.* regarding the neutral stability of the subcritical modes and the stability of a film profile featuring a single shock located in the lower half on the rising side of the cylinder. O'Brien (2002*b*) extends the lubrication model to higher order in the dimensionless film thickness (including the small effects of the variation of the film pressure across the film thickness and surface tension) and studies the stability of steady two-dimensional solutions to two-dimensional disturbances. Although surface tension prevents instability in most cases, negative diffusion in the upper half of the cylinder causes instability when higher-order effects are strong enough. O'Brien carefully discusses a range of profiles featuring single and multiple shocks, and examines their stability in terms of kinematic-wave theory. Benilov, O'Brien & Sazonov (2003) study novel explosive instabilities using model equations loosely related to those governing thin-film rimming flow. Their system admits infinitely many neutrally stable harmonic modes, but has non-harmonic solutions that develop singularities in finite time.

Motivated by applications in rapidly rotating machinery, Villegas-Díaz, Power & Riley (2003) generalize the lubrication model of the rimming-flow problem to incorporate the effect of a constant applied surface shear and undertake a comprehensive study of both sub- and supercritical solutions and their stability. Using kinematic-wave theory, they describe novel weak solutions where the stable surface profile may feature a shock at any location around the cylinder. Black (2002) also studies this problem, generalizing to both exterior and interior flows. He calculates (using lubrication theory) the maximum load of liquid that can be supported on the outside of a cylinder, and the study includes an analysis of single-shock structures when the cylinder is stationary.†

In this work we develop a higher-order lubrication theory for the problem considered by Villegas-Díaz *et al.* (2003). Our principal aim is to address issues regarding the existence and uniqueness of steady two-dimensional solutions which, according to lubrication theory, feature shocks. In particular, we include the effects of surface tension at leading order and take into account higher-order effects produced by gravity. We find, by analytical and numerical means, a set of feasible steady two-dimensional solutions that fit within a rational asymptotic framework. Having identified mathematically feasible solutions, we study their linear stability. Though many of the observed experimental patterns are truly three-dimensional, a number of them represent instabilities of two-dimensional profiles that feature a ridge, i.e. a local steepening of the fluid profile. Thus our restricting attention to two-dimensional studies is justifiable and a sensible initial step.

The plan of this paper is as follows. In § 2, we describe the governing system of equations, which, closely following the style of Ashmore *et al.*, are developed asymptotically in the Appendices by assuming that the film has small aspect ratio. In § 3, we describe possible steady two-dimensional solutions of the lubrication model and use analytical techniques to investigate the smoothing effects of gravity and surface tension on the profiles featuring shocks. This process identifies those structures that are asymptotically consistent and hence mathematically feasible. In § 4, we describe our numerical method, while, in § 5, we present computed steady two-dimensional (weak) solutions and, in § 6, study their linear stability. Finally in § 7, we present our conclusions.

† Three months after this paper was submitted, Professor Wilson sent us a preprint, Wilson, Duffy & Black (2004), reporting on an independent study which contains work reported in Black's thesis and which overlaps with aspects of ours.

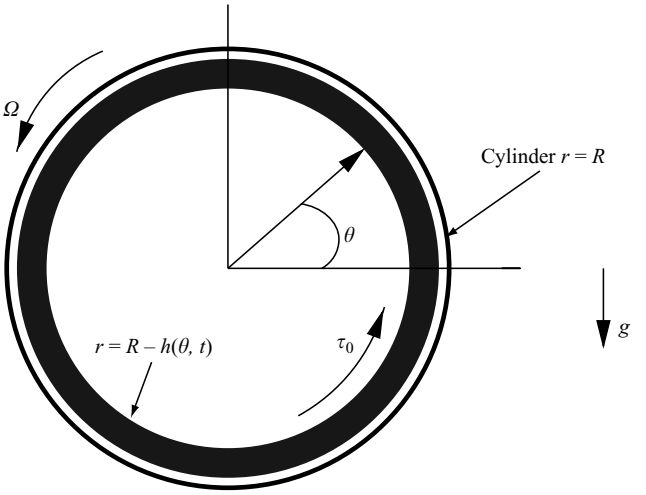

FIGURE 1. Definition sketch of the basic configuration.

2. Governing equations

Free-surface viscous flow in a partially filled circular cylinder rotating about its horizontal axis in a vertical gravitational field is considered. As in most previous studies, flow variations in the axial direction are neglected and plane polar coordinates r, centred on the cylinder axis, and θ, where $0 \leqslant \theta < 2\pi$ measured anticlockwise from the horizontal (figure 1), are employed.

Incompressible viscous fluid of thickness $h(\theta, t)$, density ρ, viscosity ν and surface tension σ flows on the interior of an infinite circular cylinder of radius R rotating anticlockwise about its horizontal axis with angular velocity Ω in a gravitational field $\boldsymbol{g} = -g\boldsymbol{j}$, where $\boldsymbol{j}$ is a unit vector pointing vertically upwards and g is the acceleration due to gravity. On assuming that thermophysical properties of the fluid are all uniform, the velocity, $\boldsymbol{u} = (u, v)$, and pressure, p, satisfy the continuity and Navier–Stokes equations

$$\nabla \cdot \boldsymbol{u} = 0, \tag{2.1}$$

$$\boldsymbol{u} \cdot \nabla \boldsymbol{u} = -\rho^{-1}\nabla p + \nu \nabla^2 \boldsymbol{u} + \boldsymbol{g}. \tag{2.2}$$

In this investigation, the effects of surface tension and of a constant shear stress acting at the free surface are studied, thus 2π-periodic solutions are sought such that

$$\boldsymbol{u} = \Omega R \boldsymbol{e}_\theta \quad \text{at } r = R, \tag{2.3}$$

$$\boldsymbol{n} \cdot \boldsymbol{T} = -p_a \boldsymbol{n} - \sigma \kappa \boldsymbol{n} + T_a \boldsymbol{t} \quad \text{at } r = R - h(\theta, t), \tag{2.4}$$

where $\boldsymbol{T}$ is the stress tensor, $\boldsymbol{t}$ ($\boldsymbol{n}$) is the unit tangential (normal) vector to the interface (directed away from the fluid), p_a is the constant pressure outside the film, κ is the curvature of the free surface and T_a is the applied constant surface stress.

The study concentrates on the case when the so-called filling fraction A is small, where

$$\pi R A = \int_0^{2\pi} \left[h(\theta, t) - \frac{h(\theta, t)^2}{2R} \right] \mathrm{d}\theta. \tag{2.5}$$

Thus if h_0 is taken as a typical film thickness such that $h_0 \ll R$, it could conveniently be defined by

$$h_0 = \frac{1}{2\pi}\int_0^{2\pi} h(\theta, t)\,\mathrm{d}\theta.$$

The details of the derivation of the asymptotic form of the governing system as $\delta = h_0/R \to 0$ are relegated to the Appendices. To $O(\delta)$, the dimensionless profile height h is governed by an evolution equation involving the dimensionless flux q

$$(1-\delta h)\frac{\partial h}{\partial t} + \frac{\partial q}{\partial \theta} = 0, \tag{2.6}$$

where

$$\begin{aligned} q = {} & h + \tfrac{1}{2}\gamma h^2 - \tfrac{1}{3}h^3\left(\Gamma\cos\theta - B^{-1}\frac{\partial}{\partial\theta}\left(h + \frac{\partial^2 h}{\partial\theta^2}\right)\right) \\ & + \delta\left[-\tfrac{1}{2}h^2 - \tfrac{5}{6}\gamma h^3 + \tfrac{1}{2}\Gamma h^4\cos\theta + \tfrac{1}{3}\Gamma h^3\frac{\partial h}{\partial\theta}\sin\theta\right. \\ & \left. - \tfrac{1}{6}h^4 B^{-1}\frac{\partial}{\partial\theta}\left(h + \frac{\partial^2 h}{\partial\theta^2}\right) + \tfrac{1}{3}h^3 B^{-1}\frac{\partial}{\partial\theta}\left(h^2 + 2h\frac{\partial^2 h}{\partial\theta^2} + \tfrac{1}{2}\left(\frac{\partial h}{\partial\theta}\right)^2\right)\right]. \end{aligned} \tag{2.7}$$

This system contains the three dimensionless groups $\gamma = T_a\delta/\mu\Omega$, $\Gamma = gh_0^2/\nu\Omega R$ and $B^{-1} = \sigma\delta^3/\Omega\mu R$.

When $\gamma = 0$, (2.6) and (2.7) reduce to the forms derived by Ashmore *et al.* (2003) when differences in notation and minor typographical errors (in Ashmore *et al.* (2.8), the expression for κ_1, is in error and in their equation (2.13) the coefficient of $\mathrm{d}\kappa_1/\mathrm{d}\theta$ should involve 1/3, not 1/6) are taken into account. Note that Tirumkudulu & Acrivos (2001) confirm the great utility of asymptotic representations, such as those derived in the Appendices, by demonstrating the close agreement of the resulting film profiles with those obtained experimentally, as well as by numerically solving the Stokes equations.

Neglecting $O(\delta)$ and surface-tension terms corresponds to the classical lubrication limit; the system (2.6), (2.7) with $\delta = B^{-1} = 0$ is termed the 'lubrication model'.

3. Lubrication model ($\delta = 0$ and $B^{-1} = 0$)

For definiteness, we take the characteristic film thickness $h_0 = \sqrt{\nu\Omega R/g}$ so that $\Gamma = 1$ througout this study (the slight loss in generality is covered by the studies of Revallo & Riley (2004) for $\Gamma \ll 1$, and of Ashmore *et al.* (2003) for $\Gamma \gg 1$). The steady-state solutions for the lubrication model, with negligible surface shear stress ($\gamma = 0$), that are immediately relevant to the rimming-flow problem considered herein are well known and were originally investigated by Moffatt (1977) and subsequently revisited by Johnson (1988), Benjamin *et al.* (1993), Wilson & Williams (1997) and O'Brien & Gath (1998). Moffatt describes the solutions in terms of the value of the flux q and a dimensionless mean film thickness $\bar{h}$ defined by

$$\bar{h} = \frac{1}{2\pi}\int_0^{2\pi} h(\theta, t)\,\mathrm{d}\theta,$$

which is effectively a measure of the filling fraction, since

$$A = \frac{\delta}{\pi}\int_0^{2\pi}\left(h(\theta, t) - \frac{\delta}{2}h(\theta, t)^2\right)\mathrm{d}\theta,$$

and $A = 2\delta\bar{h}$ to leading order in δ. When $q < 2/3$, there is a single bounded neutrally stable film profile which is smooth and completely wets the cylinder's surface. This profile has vertical symmetry, its thickness being a maximum at $\theta = 0$, i.e. at the equator on the rising side of the cylinder, and a minimum at the point diagonally opposite. There are two other profiles: a C^∞-profile which is totally negative and physically infeasible, and an unbounded profile consisting of two disconnected positive and negative branches. A larger filling fraction leads to a new smooth profile with larger mean film thickness and flux until $\bar{h} = \bar{h}_{1c} = 0.7071$ and $q = 2/3$, when the profile remains symmetric and continuous, but loses smoothness, developing a corner at $\theta = 0$ with a discontinuous slope. At this point the positive unbounded branch effectively coalesces with the physical branch. For $q = 2/3$ and $\bar{h}_{1c} < \bar{h} < \bar{h}_{2c} = 1.1023$, no continuous profile exists, but asymmetric stable (weak) solutions can be constructed from the two solution branches by introducing a shock in the fourth quadrant (i.e. by jumping between the two branches). Benjamin *et al.* were the first to highlight and calculate the upper bound corresponding to h_{2c}; note that (i) their value is 1.1067 and is at slight variance with ours; (ii) this particular type of upper bound applies throughout this study but is left implicit, i.e. we have not re-calculated it for each and every case.

The possible steady-state solutions of (2.7) with $\delta = 0$ and non-zero surface stress ($\gamma \neq 0$) were investigated independently by Villegas-Díaz *et al.* (2003) and by Black (2002). Broadly speaking, the results in the cases of $\gamma \geqslant 0$, $q > 0$ and $\gamma < 0$, $q < 0$ are qualitatively similar to those described above. However, when $\gamma < 0$ and $q > 0$, considerable differences are observed between the cases with zero and with non-zero surface stress.

3.1. *The surface shear stress and the azimuthal flux in opposite directions: $\gamma < 0$ and $q > 0$*

This is the case with the richest dynamics. Generally, there are now two positive C^∞-profiles and a third disjoint profile with unbounded positive and negative branches (cf. figure 3). These two continuous profiles allow, at least in principle, the existence of shock structures at any location around the cylinder. This contrasts with the pure rotation case when a stable shock can exist only in the fourth quadrant, i.e. on the lower half of the rising side of the cylinder.

For a given γ, there are two critical fluxes corresponding to the existence of corners:

$$q_c^0 = h_c(0)\left(\tfrac{2}{3} + \tfrac{1}{6}\gamma h_c(0)\right), \tag{3.1}$$

and

$$q_c^\pi = h_c(\pi)\left(\tfrac{2}{3} + \tfrac{1}{6}\gamma h_c(\pi)\right), \tag{3.2}$$

at $\theta = 0$ (cf. figure 3*a*) and $\theta = \pi$ (cf. figure 3*b*), respectively; h_c denotes the height of the film at the corner. The existence of these two critical fluxes for a given value of $\gamma < 0$ implies that there are two possible branches of physically sensible solutions with different values of the critical flux. In order to analyse all the possible profiles, it is convenient to refer to specific regions of parameter space. In figure 2, we show regions of γ, q-space with boundaries given by the graphs of the critical fluxes as functions of γ, together with illustrations of the various profiles that can occur when a fully wetting solution exists. There are three main regions in which the solutions exhibit qualitatively different behaviours. Noting that $q_c^0 = q_c^\pi = 0.2068$ when $\gamma = \gamma_b = -2.149139$, region I is defined by the set of points $\{(\gamma, q): -4/\sqrt{3} < \gamma < \gamma_b, 0 < q \leqslant q_c^\pi$ and $\gamma \geqslant \gamma_b, 0 < q \leqslant q_c^0\}$, region II by $\{(\gamma, q): -4/\sqrt{3} > \gamma, q_c^\pi \leqslant q < 0\}$ and region III by

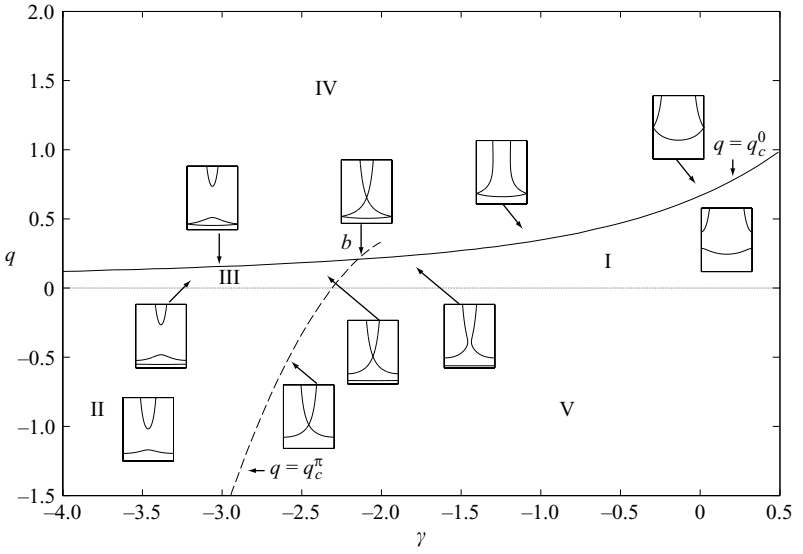

FIGURE 2. q versus γ showing regions I, II, III, IV and V and the critical curves $q = q_c^0$ (solid curve) and $q = q_c^\pi$ (dashed curve). The insets illustrate the various profiles present in each region.

$\{(\gamma, q): \gamma < -4/\sqrt{3}, 0 < q \leqslant q_c^0$ and $-4/\sqrt{3} < \gamma < \gamma_b, q_c^\pi \leqslant q \leqslant q_c^0\}$. In the remainder of parameter space (regions IV and V) there are no steady fully wetting two-dimensional solutions.

Thus the region of physical interest in γ, q-space with $\gamma q < 0$ consists of that part of region I where $\gamma < 0$ and $q > 0$, and region III. Within region I, the situation is a simple development of the Moffatt case described in § 3. The only qualitative change is that, as γ decreases through zero (with q fixed), the unphysical upper branch develops a turning point where $\mathrm{d}\theta/\mathrm{d}h = 0$ and the upper branch exists for $|\theta| < \theta_{tp}$, say. This occurs at $(\gamma, q) = (\gamma_{tp}, q_c^0)$, say, along the critical curve.

When (γ, q) reaches the dashed curve in figure 2, the turning point becomes a corner and as γ decreases further, so that the parameter values lie in region III, the upper curve above the turning point detaches leaving behind a completely wetting profile and creating a new unphysical, unbounded part. Within region III, we have three real positive profiles: (i) smooth with $h < h_c(0)$; (ii) smooth with $h_c(0) < h < h_c(\pi)$; and (iii) a disjoint profile with unbounded positive and negative branches, the positive branch having minimum height $h(\pi) > h_c(\pi)$. Therefore in this region, we always have two completely wetting film profiles corresponding to different mean film thicknesses, but associated with the same flux. When $q = q_c^0$, the two wetting profiles have a common height at $\theta = 0$, but differing mean film thicknesses, and the positive unbounded branch is not attached to the other two branches (see figure 3*a*). On the other hand, when $q = q_c^\pi$ (see figure 3*b*), the two wetting branches are disjoint, but the positive unbounded branch is attached to the upper wetting branch at $\theta = \pi$. Figure 3(*c*) illustrates the special case when the condition $q = q_c^0 = q_c^\pi$ is satisfied. In this case, the two wetting profiles are joined at the origin, while the upper wetting branch is joined with the unbounded branch at $\theta = \pi$. For values of $q \neq q_c^0$ or q_c^π, the three branches are completely disjoint.

Now, in principle, solutions featuring shocks may be constructed by joining positive branches of the leading-order solutions in an appropriate way. This may involve single

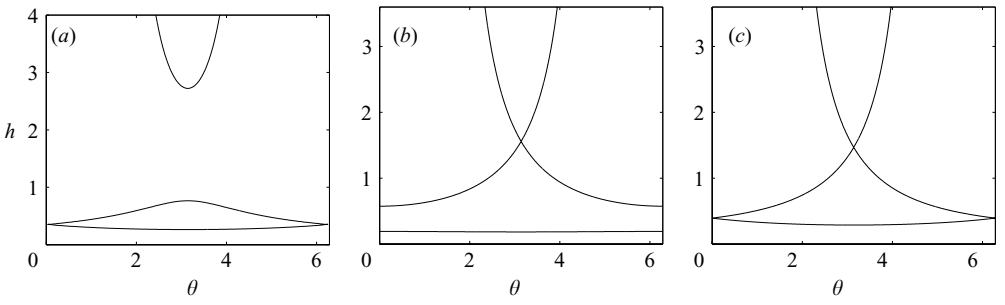

FIGURE 3. The film profiles for the cases with $\delta = 0$, $B^{-1} = 0$ and (*a*) $q = q_c^0 = 0.1825$ and $\gamma = -2.5$; (*b*) $q = q_c^\pi = 0.148$ and $\gamma = -2.2$; (*c*) $q = q_c^0 = q_c^\pi = 0.2068$ and $\gamma = -2.149139$.

shocks, as discussed by Villegas-Díaz *et al.* or multiple shocks (Johnson 1988), which have not previously been fully explored in the particular context of rimming flows. Observe that, for fixed values of the mean film thickness and flux, there are infinitely many steady-state completely wetting film profiles featuring multiple shocks (i.e. crenellated structures). One of the main objectives of this study is to analyse how this non-uniqueness is moderated by the effects of gravitational and surface-tension smoothing. Furthermore, by investigating the stability of such steady solutions, we shall determine which of them are physically realizable.

In the present study, two questions are addressed. (i) Does (2.7) possess an asymptotic structure that accommodates regions of rapid variation that match onto smooth outer solutions? (ii) Are the solutions (linearly) stable and hence physically realizable? Aspects of the first question when $\gamma = 0$ have previously been considered, for example by Johnson (1988), and Benjamin *et al.* (1993), and in more detail by Wilson & Williams (1997) and Wilson, Hunt & Duffy (2002). In contrast, the question of stability of weak solutions has received much less attention (see Villegas-Díaz *et al.* 2003).

Before presenting steady-state profiles, we investigate some of the detail of the asymptotic structure of the solutions featuring shocks. Smoothing of the shock structure may be achieved by incorporating effects neglected in the lubrication model. Two smoothing mechanisms are possible within the current model, gravity and surface tension. Johnson (1988) was the first to discuss gravitational smoothing; while Wilson & Williams (1997) presented the first substantial analysis of surface-tension smoothing. The analysis is straightforward (see below): we simply identify the derivative terms that become significant in the inner region surrounding the shock and rescale to bring these into balance (cf. Black 2002, who has independently studied this problem).

3.2. *Gravitational smoothing of shocks*

Suppose first that surface tension is neglected, so that (2.7) reduces to

$$q = h + \tfrac{1}{2}\gamma h^2 - \tfrac{1}{3}h^3\cos\theta + \delta\left[-\tfrac{1}{2}h^2 - \tfrac{5}{6}\gamma h^3 + \tfrac{1}{2}h^4\cos\theta + \tfrac{1}{3}h^3\frac{\partial h}{\partial\theta}\sin\theta\right]. \quad (3.3)$$

When $\delta = 0$, this equation has three roots, denoted by h_1, h_2 and h_3 say, which can be written down explicitly using the Cardano formulae (Revallo & Riley 2004). Since we are analysing a situation when shocks may occur, at least two, and hence all three, roots may be taken to be real. On setting $\theta = \theta_s + \delta\phi$ in the inner region around a shock located at $\theta = \theta_s (\neq 0 \text{ or } \pi)$ and taking $h(\theta) \equiv H(\phi) = O(1)$ as $\delta \to 0+$, (3.3)

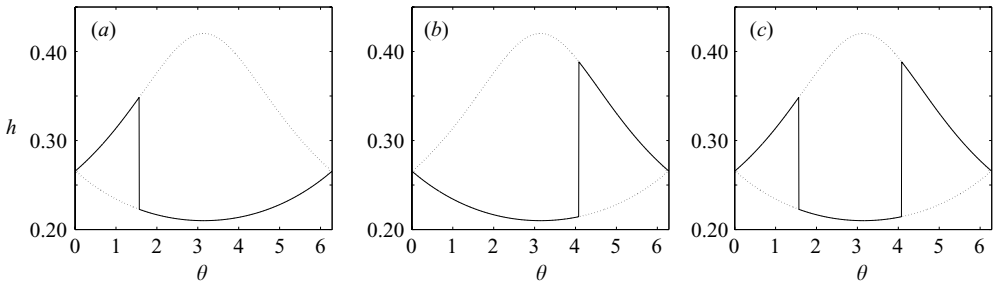

FIGURE 4. Examples of possible shock structures in the critical case $q = q_c^0 = 0.1359$, $\gamma = -3.5$, $\delta = 0$, $B^{-1} = 0$: (*a*) $\bar{h} = 0.2432$, (*b*) $\bar{h} = 0.2584$, (*c*) $\bar{h} = 0.2740$.

gives, at leading order,

$$\cot\theta_s \frac{\mathrm{d}\phi}{\mathrm{d}H} = \frac{H^3 \cos\theta_s}{3\left(q - H - \frac{1}{2}\gamma H^2 + \frac{1}{3}H^3\cos\theta_s\right)} \tag{3.4}$$

$$\approx \frac{H^3}{(H-h_1)(H-h_2)(H-h_3)}. \tag{3.5}$$

Equation (3.5) has an implicit solution, satisfying $H(0) = h_s$, given by

$$\phi\cot\theta_s = -h_s + H + \frac{h_1^3}{(h_2-h_1)(h_3-h_1)}\log\left|\frac{H-h_1}{h_s-h_1}\right| + \frac{h_2^3}{(h_3-h_2)(h_1-h_2)}\log\left|\frac{H-h_2}{h_s-h_2}\right| + \frac{h_3^3}{(h_1-h_3)(h_2-h_3)}\log\left|\frac{H-h_3}{h_s-h_3}\right|. \tag{3.6}$$

This result provides the key to determining which shock structures are mathematically feasible. To illustrate the nature of the mathematical argument, suppose that the height at one end of the shock is h_2. In the limit $H \to h_2$,

$$\phi\cot\theta_s \sim \frac{h_2^3}{(h_3-h_2)(h_1-h_2)}\log\left|\frac{H-h_2}{h_s-h_2}\right|, \to -\mathrm{sign}[(h_3-h_2)(h_1-h_2)]\infty. \tag{3.7}$$

If $\mathrm{sign}[(h_3-h_2)(h_1-h_2)] < 0$, then $\phi \to +\infty$ $(\theta > \theta_s)$ when $0 < \theta_s < \pi/2$ and $\pi < \theta_s < 3\pi/2$. In other words, this end of the shock must be approached in a clockwise direction along the branch on which $h \to h_2$ as $\theta \to \theta_s+$ in order to allow asymptotic matching. On the other hand, if the sign were positive, this end must be approached from the anticlockwise direction. Systematic application of this form of argument indicates the possible shock structures.

When $q = q_c^0$, the local analysis suggests that forward-facing shocks (height decreases as θ increases) are feasible in the upper half of the cylinder, i.e. the first and second quadrants $(0 < \theta_s < \pi)$, and rearward-facing shocks in the lower half, i.e. the third and fourth quadrants $(\pi < \theta_s < 2\pi)$. In this case, for a mean film thickness in excess of that of the lower wetting branch, $\bar{h}^l$, but less than $\bar{h}^m = (\bar{h}^u + \bar{h}^l)/2$, the mean of the mean film thicknesses of the upper and lower wetting branches, it is feasible to have three qualitatively different shock profiles. There can be a profile with a single forward- or a single rearward-facing shock, or a profile featuring a combination of them, i.e. a double-shock structure. The possibilities are illustrated in figure 4. For larger mean film thicknesses that remain less than that of the upper branch $(\bar{h}^u)$, only film profiles with a double-shock structure are feasible. On the other hand, for

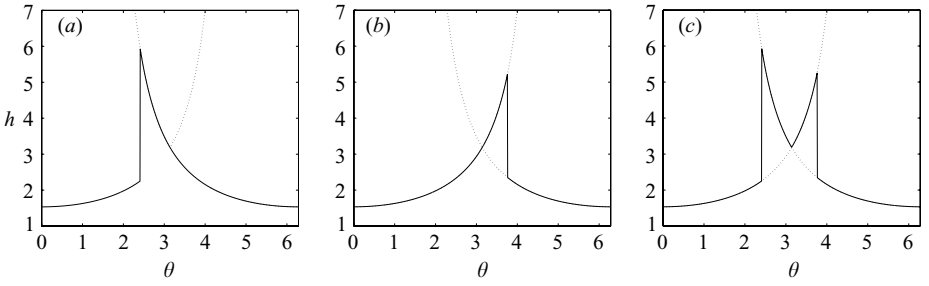

FIGURE 5. Three possible shock structures at the critical point $q = q_c^{\pi} = -3.7976$, $\gamma = -3.5$, $\delta = 0$, $B^{-1} = 0$: (a) $\bar{h} = 2.1449$, (b) $\bar{h} = 2.0889$, (c) $\bar{h} = 2.2770$.

mean film thicknesses larger than that of the upper branch, it is feasible to have a film profile featuring a double-shock structure between the upper wetting branch and a detached unbounded one, with the rearward-facing shock in the second quadrant ($\pi/2 < \theta_s < \pi$) and the forward-facing one in the third quadrant ($\pi \leqslant \theta_s < 3\pi/2$).

When $q = q_c^{\pi}$, shocks can, in principle, be found between the upper wetting branch and the unbounded branch. In this case, the local analysis indicates the feasibility of rearward-facing shocks in the second quadrant ($\pi/2 < \theta_s < \pi$) and forward-facing shocks in the third quadrant ($\pi \leqslant \theta_s < 3\pi/2$). As before, film profiles can feature single- or double-shock structures (see figure 5). In this case, it is also possible to have a film profile with a double-shock structure between the detached upper and lower wetting branches, with a forward-facing shock in the upper half of the cylinder and a rearward-facing one in the lower half.

When $q = q_c^0 = q_c^{\pi}$, any of the profiles described above are feasible.

When q is different from any of the above critical values, it is feasible to have a double-shock structure between the two (detached) wetting branches, with a forward-facing shock in the upper half of the cylinder and a rearward-facing one in the lower half, or a double-shock structure between the detached unbounded branch and the upper wetting branch, with a rearward-facing shock in the second quadrant and a forward-facing one in the third quadrant.

In summary, the local inclusion of the 'higher-order' gravitational effect reduces the range of mathematically feasible surface profiles to those that feature single- or double-shock structures (or are smooth). No more than two shocks can appear in any of the cases considered above. Therefore the local analysis does not completely remove the non-uniqueness of solutions arising in the lubrication model, but it does limit the types of possible solution.

3.3. *Smoothing of shocks by surface tension*

Suppose now that terms of $O(\delta)$ are neglected, so that (2.7) reduces to

$$q = h + \tfrac{1}{2}\gamma h^2 - \tfrac{1}{3}h^3(\cos\theta - B^{-1}(h' + h''')), \tag{3.8}$$

and that $0 < B^{-1} \ll 1$. Setting $\theta = \theta_s + B^{-1/3}\phi$ in the inner region around a shock located at $\theta = \theta_s$ and taking $h(\theta) \equiv H(\phi) = O(1)$ as $B^{-1} \to 0+$, (3.8) becomes at leading order

$$\frac{\mathrm{d}^3 H}{\mathrm{d}\phi^3} = \frac{3}{H^3}\left(q - H - \tfrac{1}{2}\gamma H^2 + \tfrac{1}{3}H^3\cos\theta_s\right). \tag{3.9}$$

In the absence of a closed-form solution to this equation, analytical progress may be achieved by local linearization. Substituting $H = h_i + \zeta(\phi)$ into (3.9), and linearizing

about the end-point of the shock, gives

$$\frac{\mathrm{d}^3\zeta}{\mathrm{d}\phi^3} = \frac{3}{h_i^3}\left(h_i^2\cos\theta_s - \gamma h_i - 1\right)\zeta, \tag{3.10}$$

where $i = 1$, 2 or 3 according to which of the film profiles is considered (for definiteness, the roots $h = h_1$, h_2 and h_3 are taken to correspond to the heights of the lower wetting, upper wetting and unbounded branches). Integrating (3.10)

$$\zeta(\phi) = a_1\exp(\alpha_i\phi) + \exp\left(-\tfrac{1}{2}\alpha_i\phi\right)\left[a_2\cos\left(\tfrac{1}{2}\alpha_i\sqrt{3}\phi\right) + a_3\sin\left(\tfrac{1}{2}\alpha_i\sqrt{3}\phi\right)\right], \tag{3.11}$$

where the coefficients a_i are constants and α_i is given by $[3(h_i^2\cos\theta_s - 1 - \gamma h_i)/h_i^3]^{1/3}$. A more useful form of α_i is obtained by noting that, on neglecting terms of $O(B^{-1})$, differentiating (3.8) with respect to θ gives

$$\left(h_i^2\cos\theta_s - 1 - \gamma h_i\right)\left.\frac{\mathrm{d}h}{\mathrm{d}\theta}\right|_{h=h_i,\theta=\theta_s} = \tfrac{1}{3}h_i^3\sin\theta_s$$

so that $\alpha_i = [\sin\theta_s/\mathrm{d}h/\mathrm{d}\theta|_{h=h_i,\theta=\theta_s}]^{1/3}$. This enables the sign of α_i to be quickly determined by noting θ_s, the angle at which the shock occurs, and the sign of the gradient of the tangent to the profile at the shock. In this way, it can be shown that, for any position of the shock (except $\theta_s = 0, \pi$), the coefficients α_1 and α_3, corresponding to positive heights h_1 and h_3, are always negative while α_2 corresponding to h_2, is always positive. Suppose α_i is negative, then to keep ζ bounded as $\phi \to -\infty$ ($\theta < \theta_s$) we must have $a_1 = 0$; for boundedness as $\phi \to \infty$ ($\theta > \theta_s$) we must have $a_2 = a_3 = 0$. In this latter case ($\phi \to \infty$), the approach to the shock is monotonic and, in general, there would be insufficient freedom in the coefficients to effect local matching. In the former case ($\phi \to -\infty$), the approach is oscillatory and it is likely that matching could be effected, thus making the existence of the shock plausible. Likewise, when α_i is positive, bounded solutions of (3.10) are monotonic for negative values of ϕ and oscillatory for positive values. An asymptotic shock structure seems to be plausible when the height of the surface profile has an oscillatory behaviour as the shock is approached from either side.

As before, applying this local result suggests that shocks between the wetting profiles $h = h_1$ and $h = h_2$, where $\alpha_1 < 0$ and $\alpha_2 > 0$, are feasible only when $h = h_1$ before the shock, i.e. at negative values of ϕ, and $h = h_2$ after the shock, i.e. at positive values of ϕ. Thus at the critical flux condition $q = q_c^0$ only a rearward-facing shock is plausible, as illustrated in figure 6. Similarly, a forward-facing shock between the wetting profile $h = h_2$ and the unbounded profile $h = h_3$ is plausible when $q = q_c^\pi$, as illustrated in figure 5(*b*). At the double critical point $q = q_c^0 = q_c^\pi$, the two previous single-shock cases are feasible (though the analysis is not valid for the rearward-facing shock for $\theta_s \approx \pi$), and the double-shock combination of these two shocks is also feasible (with the rearward-facing shock restricted to the upper half of the cylinder). The local analysis implies that other shock structures are not possible, since shocks are feasible only when two branches having differing sign[α] are joined in order to assure the required oscillatory behaviour. Likewise multiple-shock structures having the required oscillatory behaviour cannot be constructed for non-critical values of q.

Thus, it appears that the inclusion of surface tension removes the non-uniqueness of the lubrication model.

3.4. *Smoothing of shocks by surface tension and gravity*

When both higher-order surface-tension and gravitational effects are significant, it is the surface-tension derivative term that generally determines the inner behaviour

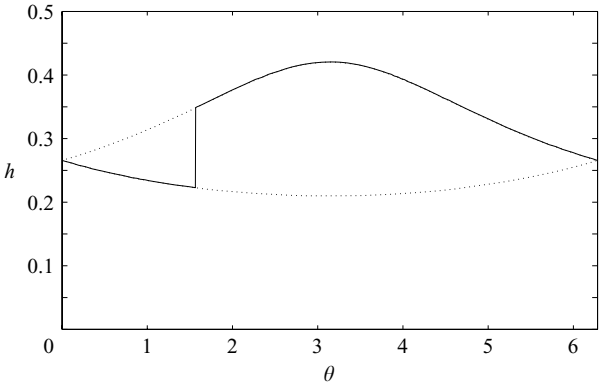

FIGURE 6. A single shock located in the second quadrant in the case $q = q_c^0 = 0.1359$, $\gamma = -3.5$, $\delta = 0$, $B^{-1} = 0$, $\bar{h} = 0.3326$.

(consistent with our assumption that $B^{-1} = O(1)$ as $\delta \to 0$) and hence the plausible shock structures. The cases are therefore summarized as:

(i) For $q = q_c^0$, $\bar{h}^l < \bar{h} < \bar{h}^u$: single rearward-facing shock joining two attached wetting branches, at any position around the cylinder.

(ii) For $q = q_c^\pi$, $\bar{h} > \bar{h}^u$: single forward-facing shock joining upper wetting branch and the unbounded branch, on the lower half of the falling side of the cylinder, i.e. $\pi < \theta < 3\pi/2$.

(iii) For $q = q_c^0 = q_c^\pi$: $(\bar{h}^l < \bar{h} < \bar{h}^u)$ single rearward-facing shock joining two wetting branches, at any position around the cylinder, except near $\theta = \pi$; $(\bar{h} > \bar{h}^u)$; single forward-facing shock joining upper wetting branch and the unbounded branch, on the lower half of the falling side of the cylinder, i.e. $\pi < \theta < 3\pi/2$.

(iv) For $q = q_c^0 = q_c^\pi$: double-shock structure with rearward-facing shock joining two wetting branches, located in top half of the cylinder and forward-facing shock joining upper wetting branch and unbounded branch, located on the lower half of the falling side of the cylinder, i.e. $\pi < \theta < 3\pi/2$.

Note that the local analyses can only suggest the form of possible solutions but not determine their exact form, since a complete asymptotic match has not been carried out. To determine further information on the effect of the smoothing terms, i.e. gravity and surface tension, a numerical study of the steady-state profiles, as well as transient processes, has been undertaken.

4. Numerical solution

To study the shock structures outlined in § 3, steady-state film profiles were found numerically by solving (2.7) for those values of q and mean film thickness $\bar{h}$, for which shocks were expected to exist. The numerical scheme was based on a fourth-order central-difference approximation of the spatial derivatives over $[0, 2\pi)$. For given values of q, γ, δ, B^{-1}, and an initial guess of the profile corresponding to the solution of the algebraic part of (2.7), the nonlinear system of algebraic difference equations was solved using the MATLAB routine solve, which is a modified Newton method.

Similarly, central differences were also used to approximate the spatial derivatives in the evolution equation (2.6) and the method of lines employed to solve the resulting system of first-order ordinary differential equations; the MATLAB routine ode15s was used as the solver.

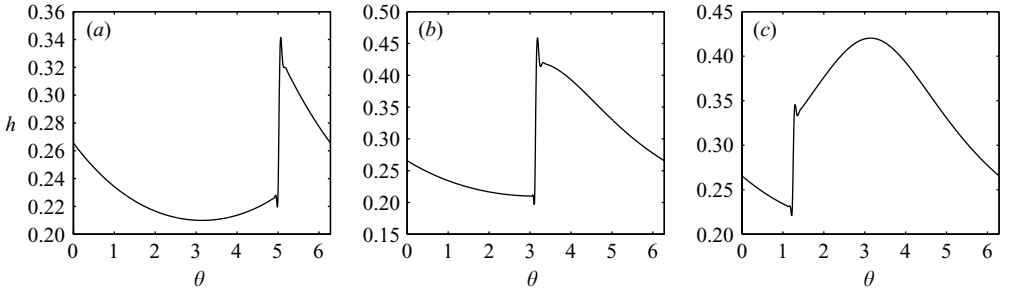

FIGURE 7. Three different computed shock profiles: $q = q_c^0 = 0.1359$, $\gamma = -3.5$, $\delta = 0.0$, $B^{-1} = 10^{-3}$ and (*a*) $\bar{h} = 0.2376$, (*b*) $\bar{h} = 0.2883$, (*c*) $\bar{h} = 0.3383$.

To validate the numerical codes, we successfully reproduced the various two-dimensional solutions reported in Benjamin *et al.* (1993) and Noakes (2001) for the case of zero surface shear. The grid-convergence of our solutions was verified by increasing the number of mesh points in regions of rapid change. For our iterative scheme, a convergence criterion of the relative error being less than 10^{-8} was satisfied in all our calculations.

5. Computed smoothed shock structures

First, we consider the effect of surface-tension smoothing, i.e. $B^{-1} \neq 0$ and $\delta = 0$. (Since $\Gamma = 1$, $B^{-1} = \sigma\delta/\rho g R^2$, therefore this situation pertains to hypothetical flows where $\sigma/\rho g R^2 \to \infty$ as $\delta \to 0$.) Assuming that the steady-state solutions of (3.8) depend smoothly on B^{-1}, it is reasonable to suppose solutions with $0 < B^{-1} \ll 1$ are close to the corresponding lubrication-model solutions. Thus, the initial guess in the computation of the smoothed structures was taken to be the solution of the cubic polynomial for the same values of q and γ. When further computations were made for incremental increases in B^{-1}, with other parameters fixed, the last converged solution was taken as the initial guess for the new value of B^{-1}.

For $q = q_c^0$ in the lubrication model, the local analysis of § 3.5 suggests that it is possible to have rearward-facing shocks, joining the two wetting branches, located anywhere around the cylinder, cf. figure 6. This is confirmed by our numerical results, see figure 7: here the initial mean film thicknesses are (*a*) $\bar{h} = 0.2376$, (*b*) $\bar{h} = 0.2883$, and (*c*) $\bar{h} = 0.3383$; $\gamma = -3.5$ and $B^{-1} = 10^{-3}$. Our numerical code failed to converge when initial profiles featuring forward-facing shocks, cf. figure 4(*a*), were used. Moreover, when initial profiles featuring multiple shocks were used, cf. figure 4(*c*), it was again not possible to find a steady-state solution. This is not altogether surprising: the multi-shock structure always comprises at least one theoretically feasible rearward-facing shock and at least one of the infeasible forward-facing shocks. These results are in complete agreement with our local analysis.

When $q = q_c^\pi$ in the lubrication model, the local analysis of § 3.5 suggests that it is possible to have forward-facing shocks, between the upper wetting branch and the unbounded branch, located only in the lower half of the cylinder, i.e. $\pi < \theta < 3\pi/2$. This was again confirmed by our computations, cf. figure 8. No other shock structure resulted from our extensive computations.

In the case of the double critical point, i.e. $q = q_c^0 = q_c^\pi$, the local analysis and the numerical results above suggest that it is feasible to have rearward-facing shocks joining the two wetting branches at any position around the cylinder except at $\theta = \pi$

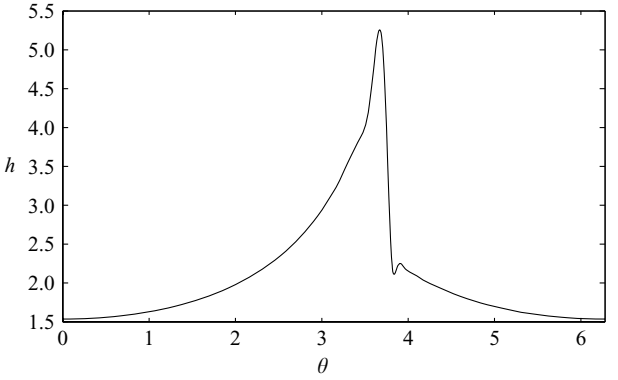

FIGURE 8. A computed single-shock profile at the critical condition: $q = q_c^{\pi} = -3.7976$, $\gamma = -3.5$, $\delta = 0.0$, $B^{-1} = 10^{-5}$ and $\bar{h} = 2.0889$.

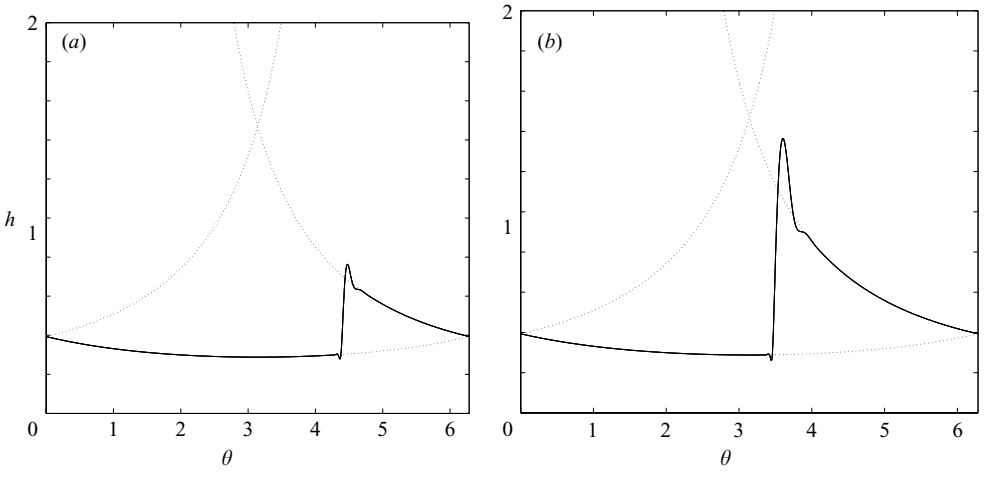

FIGURE 9. Two different computed shock profiles at the double critical point: $q = q_c^0 = q_c^{\pi} = 0.2068$, $\gamma = -2.149139$, $\delta = 0.0$, $B^{-1} = 10^{-3}$ and (*a*) $\bar{h} = 0.3736$, (*b*) $\bar{h} = 0.4939$.

(where the analysis is not valid). Our numerical solutions suggest, however, that the structure depends on the mean film thickness, in particular, when the mean film thickness is in excess of that of the lower wetting branch, the structure depends on whether the excess is less than or greater than half the difference between the respective fractions of the upper and lower wetting branches.

In the first case, specifically when $\bar{h}^l = 0.3201 < \bar{h} < 0.5156 = \bar{h}^m$, the calculations result in a rearward-facing shock in the lower half of the cylinder. Two of these rearward-facing shocks located at $\theta = 1.2\pi$ and $\theta = 1.38\pi$ are shown in figures 9(*a*) and 9(*b*), respectively. In the second case, specifically when $\bar{h}^m = 0.5156 < \bar{h} < 0.7111 = \bar{h}^u$, the additional mass in the fraction $(\bar{h} - \bar{h}^m)$ accumulates in a steady-state structure above the upper wetting branch creating a kind of double-shock structure, see figure 10(*a*) which shows the profile when $\bar{h} = 0.5944$ and $B^{-1} = 10^{-5}$. Similar surface structures have previously been observed and mathematically analysed for thin-film flows over inclined flat planes and subject to surface shear. Bertozzi, Munch & Shearer (1999) classify this type of structure as a stable interaction between compressive and undercompressive waves. According to the lubrication model in the current case, the wavespeed of infinitesimal disturbances is negative on the upper wetting branch and

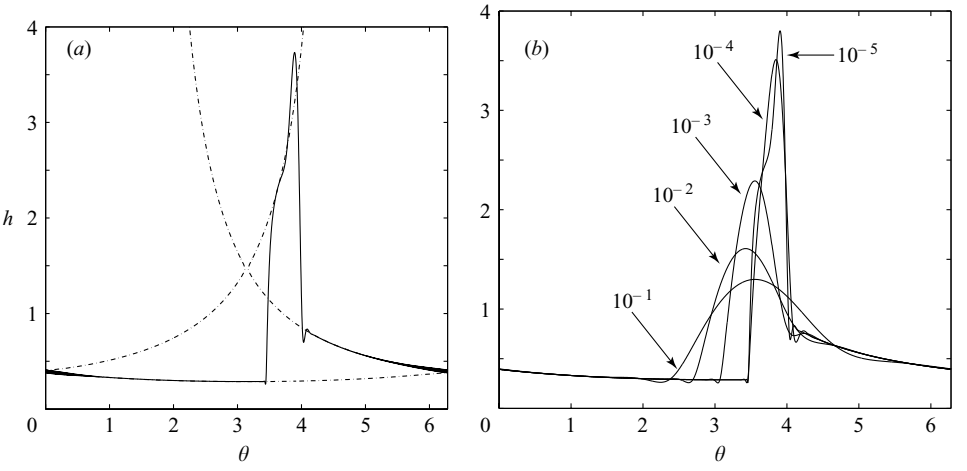

FIGURE 10. (*a*) Computed double-shock profile: $q = q_c^0 = q_c^\pi = 0.2068$, $\gamma = -2.149139$, $\delta = 0.0$, $B^{-1} = 10^{-5}$ and $\bar{h} = 0.5944 > \bar{h}^m$. (*b*) The effect of increasing the capillary number B^{-1} (values shown on the plot) on the height of the double shock in (*a*).

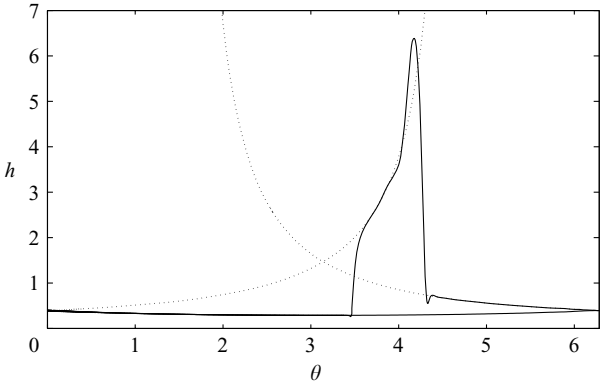

FIGURE 11. Computed double-shock profile: $q = q_c^0 = q_c^\pi = 0.2068$, $\gamma = -2.149139$, $\delta = 0.0$, $B^{-1} = 10^{-5}$, $\bar{h} = 0.7878 > \bar{h}^u$.

positive on the others, except at $\theta = 0$ and $\theta = \pi$ where it is zero. Consequently, the rearward-facing part of the double-shock structure in figure 10 is undercompressive in the sense that disturbances pass through it. On the other hand, the forward-facing part is compressive with disturbances impinging on it from both sides. Note that the steady-state solution in figure 10(*a*) avoids the singular point at $\theta = \pi$.

This new complex structure is not predicted by the local analysis (which applies only when the shock is located away from any corners in the lubrication model profiles). As B^{-1} increases, the shock structure becomes smoother, having the appearance of a single hump for larger values of B^{-1} (see figure 10*b*) showing computed profiles for $\bar{h} = 0.5944$. The surface profiles shown in figure 10 could not be obtained using the strategy outlined at the start of § 4. Instead the transient code was run for a few time steps and then its output used as the initial condition for the Newton solver. Similar complex surface profiles result when $\bar{h} > \bar{h}^u = 0.7111$, see figure 11 for the case of $\bar{h} = 0.7878$ and $B^{-1} = 10^{-5}$.

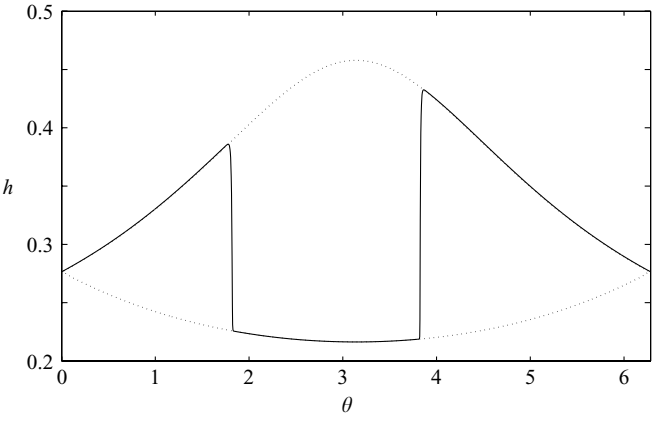

FIGURE 12. Computed double-shock profile with gravitational smoothing: $q = 0.13829 > q_c^0 = 0.1359$, $\gamma = -3.5$, $\delta = 10^{-1}$, $B^{-1} = 0.0$ and $\bar{h} = 0.29013$.

It is important to note that, even though the local analysis suggests that a forward-facing shock is feasible for $\pi < \theta_s < 3\pi/2$, we tried, but failed, to calculate forward-facing and rearward-facing steady shocks joining the the upper wetting branch and the unbounded branch shown in figure 3(*c*). It appears that, as before, any calculated solution avoids the singular point at $\theta = \pi$ and the only possible solutions with $\bar{h} > \bar{h}^u$ feature complex structures similar to that shown in figure 11. A similar structure has been obtained at parameter values $q = q_c^0$ and ($\gamma_b < \gamma < \gamma_{tp}$), i.e. when the critical point at $\theta = \pi$ in figure 11 unfolds and turning points feature.

For other values of q, we found no multiple-shock structures between the detached branches, in agreement with the local analysis. In these cases, the solution tends to a new smooth surface profile with a mean film thickness different from the initial one.

For gravitational smoothing, i.e. steady solutions of (3.3), all single- and multiple-shock structures between attached branches suggested by the local analysis (see figures 4 and 5) were reproduced numerically. As before, however, no multiple-shock structures joining detached branches were obtained, even though the local analysis supports their feasibility. Note that the initial profiles were given by the solution of the algebraic part of (3.3), rather than the solution of the cubic equation arising in the lubrication model. The algebraic part of (3.3) is given by a fourth-order polynomial and, for moderate values of δ, its solution results in a significant shift in the critical-point values, for example in the calculation of the double-shock structure in figure 12, where the original critical value $q_c^0 = 0.1359$ changes to $q_c = 0.13829$.

In cases where both gravitational and surface-tension smoothing are taken into account, the effects of surface tension dominate over gravity and the structure reflects that expected for surface-tension smoothing alone. This is true even in cases when B^{-1} was taken to be several orders of magnitude smaller than δ, for example, for $B^{-1} = 10^{-3}$ and $\delta = 10^{-1}$.

In summary, when surface tension is taken into account, the original infinity of possibilities of shocks joining real positive solutions of the lubrication model is reduced to only a few. In general, only single shocks joining attached branches are possible, the exception involves the complex double-shock structure that occurs in the cases of the double critical point and of the single critical point plus the turning point (i.e. for $\gamma_b < \gamma < \gamma_{tp}$ and $q = q_c^0$). In other words, the non-uniqueness in the lubrication

model for given values of q, γ and $\bar{h}$ seems to be completely removed by the presence of surface tension.

6. Stability analysis

From the theoretical and numerical analysis of steady solutions, we conjecture that, under real physical conditions, i.e. non-zero surface tension and gravity, only the following steady-state shock structures are possible.

(i) For $q = q_c^0$, $\bar{h}^l < \bar{h} < \bar{h}^u$: rearward-facing single shocks joining the two attached wetting branches, located at any position around the cylinder.

(ii) For $q = q_c^0$, $\gamma_b < \gamma < \gamma_{tp}$: double-shock structure may exist, depending on the mean film thickness.

(iii) For $q = q_c^\pi$, $\bar{h} > \bar{h}^u$: forward-facing single shocks joining the upper wetting branch and the unbounded branch, located only on the lower half of the falling side of the cylinder, i.e. $\pi < \theta < 3\pi/2$.

(iv) For $q = q_c^0 = q_c^\pi$, $\bar{h}^l < \bar{h} < \bar{h}^m$: rearward-facing single shocks joining the two wetting branches, located at any position in the bottom half of the cylinder, i.e. $\pi < \theta_s < 2\pi$.

(v) For $q = q_c^0 = q_c^\pi$, $\bar{h}^m < \bar{h}$: double-shock structure involving all three branches, located on the lower half of the falling side of the cylinder, i.e. $\pi < \theta < 3\pi/2$.

In order to see which of those steady shock-structures are physically realizable, i.e. sustainable under small perturbations, a numerical study of their stability is now undertaken using two alternative approaches: eigenvalue analysis and the time evolution of a localized initial disturbance. Thus the main objective is to examine the stability of steady solutions, $h_0(\theta)$ say, of the evolution system (2.6), (2.7), with respect to infinitesimal disturbances $\xi(\theta, t)$. After linearization, the equation governing the evolution of small disturbances is

$$(1-\delta h_0)\frac{\partial \xi}{\partial t} + \frac{\partial}{\partial \theta}(f_1 \xi) + \frac{\partial}{\partial \theta}\left(f_2 \frac{\partial \xi}{\partial \theta}\right) + \frac{\partial}{\partial \theta}\left(f_3 \frac{\partial^2 \xi}{\partial \theta^2}\right) + \frac{\partial}{\partial \theta}\left(f_4 \frac{\partial^3 \xi}{\partial \theta^3}\right) = 0, \quad (6.1)$$

where

$$f_1 = 1 + \gamma h_0 - h_0^2 \cos\theta + B^{-1} h_0^2 (h_0 + h_0'')' + \delta\big[-h_0 - \tfrac{5}{2}\gamma h_0^2 + 2h_0^3 \cos\theta + h_0^2 h_0' \sin\theta + B^{-1} h_0^2 \big(h_0^2 + 2h_0 h_0'' + \tfrac{1}{2}(h_0')^2\big)'\big], \quad (6.2)$$

$$f_2 = B^{-1}\tfrac{1}{3}h_0^3 + \tfrac{1}{3}\delta h_0^3 \sin\theta + \delta B^{-1}\big(\tfrac{1}{2}h_0^4 + h_0^3 h_0''\big), \quad (6.3)$$

$$f_3 = \delta B^{-1} h_0^3 h_0', \quad f_4 = B^{-1}\tfrac{1}{3}h_0^3 + \delta B^{-1}\tfrac{1}{2}h_0^4. \quad (6.4)$$

Note that these expressions are consistent with those of O'Brien (2002*b*). In the lubrication model, the evolution equation reduces to

$$\frac{\partial \xi}{\partial t} + \frac{\partial (f\xi)}{\partial \theta} = 0, \quad (6.5)$$

with

$$f = 1 + \gamma h_0 - h_0^2 \cos\theta, \quad (6.6)$$

where q is given by (2.7) with $\delta = B^{-1} = 0$, see Villegas-Díaz *et al.* (2003).

On neglecting surface-tension effects in (6.1), the evolution equation may be written

$$\frac{\partial \xi}{\partial t} + \frac{\partial}{\partial \theta}(\mathscr{F}_1 \xi) + \frac{\partial}{\partial \theta}\left(\mathscr{F}_2 \frac{\partial \xi}{\partial \theta}\right) + \mathscr{F}_0 \xi = 0, \quad (6.7)$$

where

$$\mathscr{F}_0 = \left(\frac{\delta h_0' f_2}{(1-\delta h_0(\theta))^2}\right)' - \frac{\delta h_0' f_1}{(1-\delta h_0(\theta))^2}, \tag{6.8}$$

$$\mathscr{F}_1 = \frac{f_1}{(1-\delta h_0(\theta))} - \frac{\delta h_0' f_2}{(1-\delta h_0(\theta))^2}, \tag{6.9}$$

$$\mathscr{F}_2 = \frac{f_2}{(1-\delta h_0(\theta))}. \tag{6.10}$$

Therefore the evolution of a disturbance is given by a reaction-convection-diffusion equation with a variable diffusion coefficient, $-\mathscr{F}_2$, that is negative in the upper half of the cylinder and positive in the lower half, a variable convective velocity, $-\mathscr{F}_1$ and a source term $-\mathscr{F}_0$. Thus long waves can be convected away from the region of negative diffusion before they blow-up. There will, however, always be some short waves that the negative diffusion will cause to focus and blow-up before they are convected from this critical region. This process has previously been identified as one of the main sources of instability in this type of flow, see O'Brien (2002*b*). When surface tension is taken into consideration, the strength of the negative diffusion increases (cf. (6.3)), apparently exacerbating the problem. However, positive diffusion, manifest in the f_4-term in (6.1), dominates at high wavenumber and mitigates the effects of negative-diffusion. This feature is present in the numerics of O'Brien (2002*b*) in his stability analysis of smooth film profiles (for zero surface shear, but including the stabilizing pressure correction due to the centrifugal force).

Here we consider the stability of smooth film profiles featuring regions of rapid variation (shocks). As pointed out in the previous sections, the presence of surface shear, applied in the opposite sense to the direction of the rotation of the cylinder, results in the possibilities of more complex steady-state surface profiles.

In addition to considering the evolution of initially small disturbances in order to study the linear stability of calculated steady profiles, we also determined the complex frequencies σ of travelling disturbances $\xi(\theta, t) = \chi(\theta)\,\mathrm{e}^{\sigma t}$ by computing the eigenvalues of the problem that results when ξ is substituted into (6.1) and remaining spatial derivatives discretized. Disturbances with $\mathrm{Re}\{\sigma\} < 0$, $\mathrm{Re}\{\sigma\} = 0$, $\mathrm{Re}\{\sigma\} > 0$ are stable, neutrally stable and unstable, respectively; $\mathrm{Im}\{\sigma\}$ is the frequency of the disturbance. The eigenvalue problem was solved using the MATLAB routine eig.

The eigenvalues of disturbances to the shock profiles shown in figures 7 to 11, which are representative of the totality of the possible cases when $\delta = 0$, were found to be complex with negative real part, i.e. the disturbances comprise travelling waves with attenuating wave amplitude. Thus the steady-state profiles are linearly stable to this type of disturbance. Figure 13(*a*) shows the calculated eigenvalues for the base profile shown in figure 13(*b*), a profile with a rearward-facing single shock in the upper quadrant of the rising side of the cylinder: $\gamma = -3.5$, $q = q_c^0 = 0.1359$, $\delta = 0$, $B^{-1} = 10^{-3}$ and $\bar{h} = 0.3458$. The corresponding results for a profile featuring a double-shock structure are presented in figure 14: $\gamma = -2.149139$, $q = q_c^0 = q_c^\pi = 0.2068$, $\delta = 0$, $B^{-1} = 10^{-3}$ and $\bar{h} = 0.5944$.

When both surface-tension and gravitational smoothing effects are included, we generally observe similar stable behaviour to these cases. However, as $B^{-1} \to 0$, for fixed δ, there is a loss of stability via a Hopf bifurcation. This is illustrated in figure 15 for a profile featuring a rearward-facing single shock. Here $\gamma = -3.5$, $\delta = 0.01$, and $q = q_c^0 = 0.1359$, $\bar{h} = 0.29013$, with decreasing values of B^{-1}: (*a*) 10^{-3}, (*b*) 10^{-4} and (*c*) 10^{-5}; the profile in (*d*) corresponds to case (*a*). As can be observed, for $B^{-1} = 10^{-5}$,

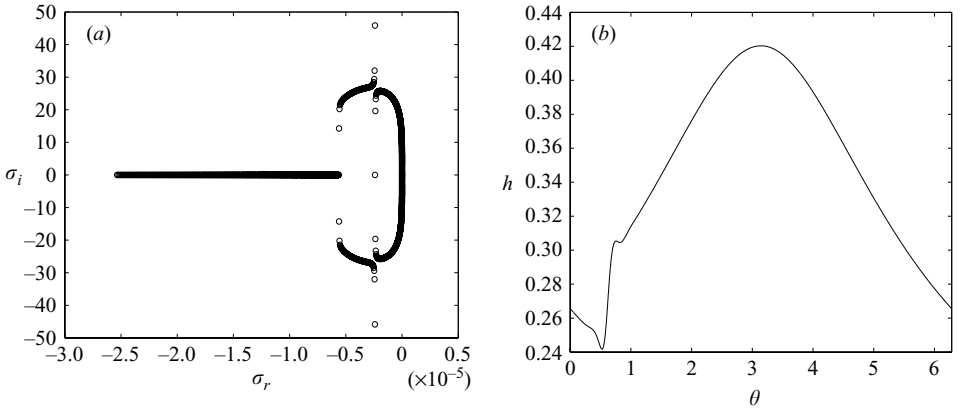

FIGURE 13. (*a*) Computed eigenvalue spectrum and (*b*) shock profile: $q = q_c^0 = 0.1359$, $\gamma = -3.5$, $\delta = 0.0$, $B^{-1} = 10^{-3}$ and $\bar{h} = 0.3458$.

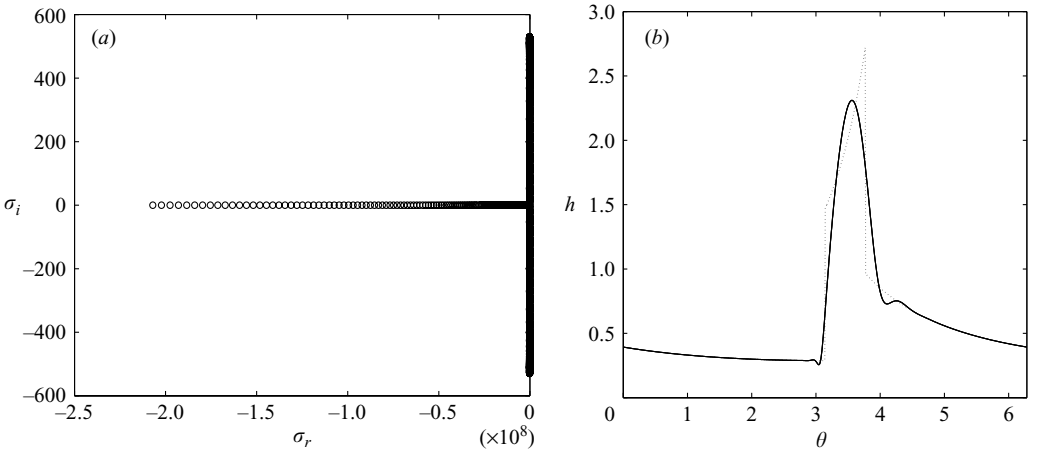

FIGURE 14. (*a*) Computed eigenvalue spectrum and (*b*) shock profile corresponding to the double-critical point: $q = q_c^0 = q_c^\pi = 0.2068$, $\gamma = -2.149139$, $\delta = 0.0$, $B^{-1} = 10^{-3}$ and $\bar{h} = 0.5944$.

some of the eigenvalues have moved into the right-hand side of the complex plane, the positive real part implying travelling waves with growing wave amplitude.

In order to investigate how an initially small disturbance develops in time, we used the method of lines to solve the linear evolution equation (6.1). Of particular interest is how the disturbances evolve as they approach a shock. In figure 16(*a–c*), the time evolution of an initially sinusoidal wave of period 2π, $\xi(\theta, 0) = 0.01 \sin\theta$, is shown for a profile with a rearward-facing single shock. The initial profile is shown in figure 16(*d*): $\gamma = -2.5$, $\delta = 0.0$, $q = 0.1825$, $B^{-1} = 10^{-3}$ and $\bar{h} = 0.46$. Initially the disturbance focuses towards the shock, accompanied by a significant increase in the wave height and a reduction in the wavelength, see figure 16(*a*), as expected from the study of the lubrication problem by Villegas-Díaz *et al.* (2003). This focusing results in the formation of a pointed spike at the position of the original shock. After the maximum height is reached, surface tension damps the disturbance until a stable state is achieved when the original perturbation is completely absorbed by the shock, see figure 16(*b, c*); figure 16(*c*) shows both the approach to the terminal state and the

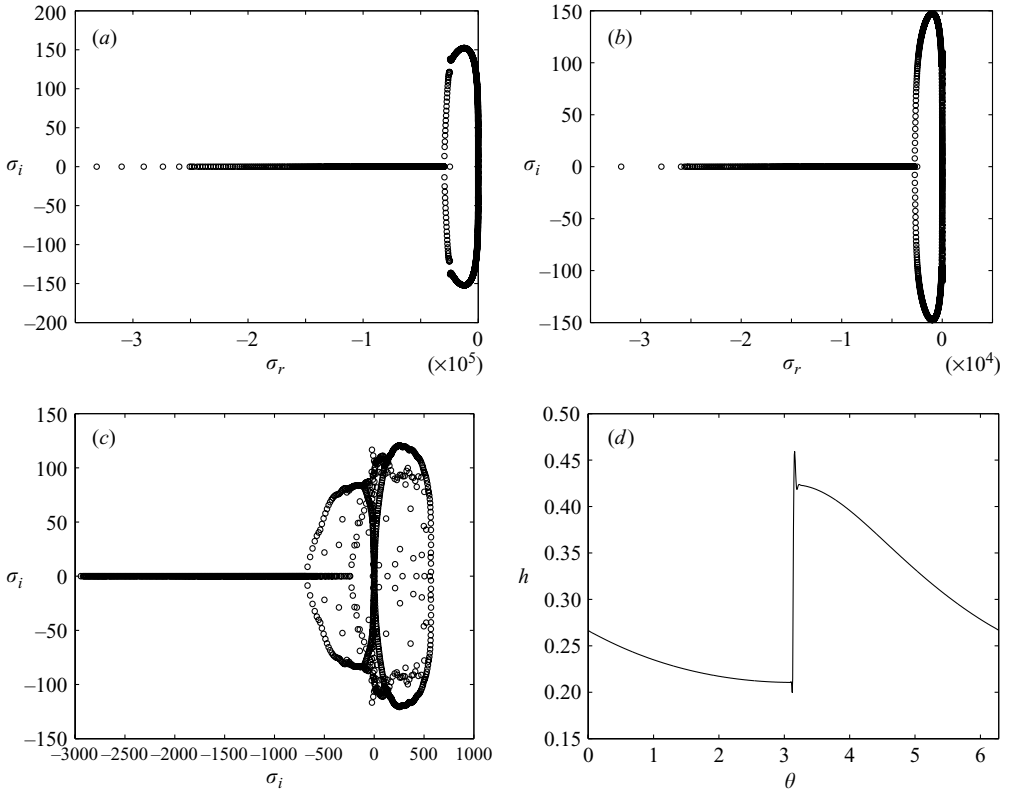

FIGURE 15. Eigenvalue spectrum: $q = 0.1359 \approx q_c^0$, $\gamma = -3.5$, $\delta = 10^{-2}$, $\bar{h} = 0.29013$, and (*a*) $B^{-1} = 10^{-3}$, (*b*) $B^{-1} = 10^{-4}$, (*c*) $B^{-1} = 10^{-5}$; (*d*) the shock profile in case (*a*).

initial disturbance (dotted curve). As, during the focusing process, the wave amplitude reaches a significant magnitude which is outside the range of validity of the linear approximation, we repeated the simulation using the nonlinear system (2.6), (2.7). The results from the nonlinear transient problem were qualitatively identical to the linear one, with a smaller maximum wave amplitude during the focusing process.

Similar focusing and concurrent mitigation effects were observed when the evolution of perturbations to profiles with double-shock structures was analysed. During the focusing process, two spikes instead of one are formed at the shock positions (see figure 17). This figure shows the corresponding evolution of a sinusoidal disturbance of period 2π on the base profile displayed in figure 17(*d*), $\gamma = -2.149139$, $\delta = 0$, $q = 0.2068$, $B^{-1} = 10^{-3}$ and $\bar{h} = 0.5944$.

A similar evolution process, for profiles with either single and double shocks, occurs when sinusoidal perturbations with higher wavenumbers are considered. It is noteworthy that the maximum amplitude of the spikes decreases as the wavenumber of the initial disturbance increases. From this analysis, we conclude that not only does the inclusion of surface tension make the solution to a given problem unique, but also stabilizes the possible shock profiles.

The results confirm the filling mechanism that we proposed in our previous work, Villegas-Díaz *et al.* (2003), namely, for fixed values of γ and $q = q_c^0$, it is possible to have a stable transition from the thinner wetting surface profile $h = h_1$ to the thicker one $h = h_2$ by the added mass being absorbed at a single rearward-facing shock

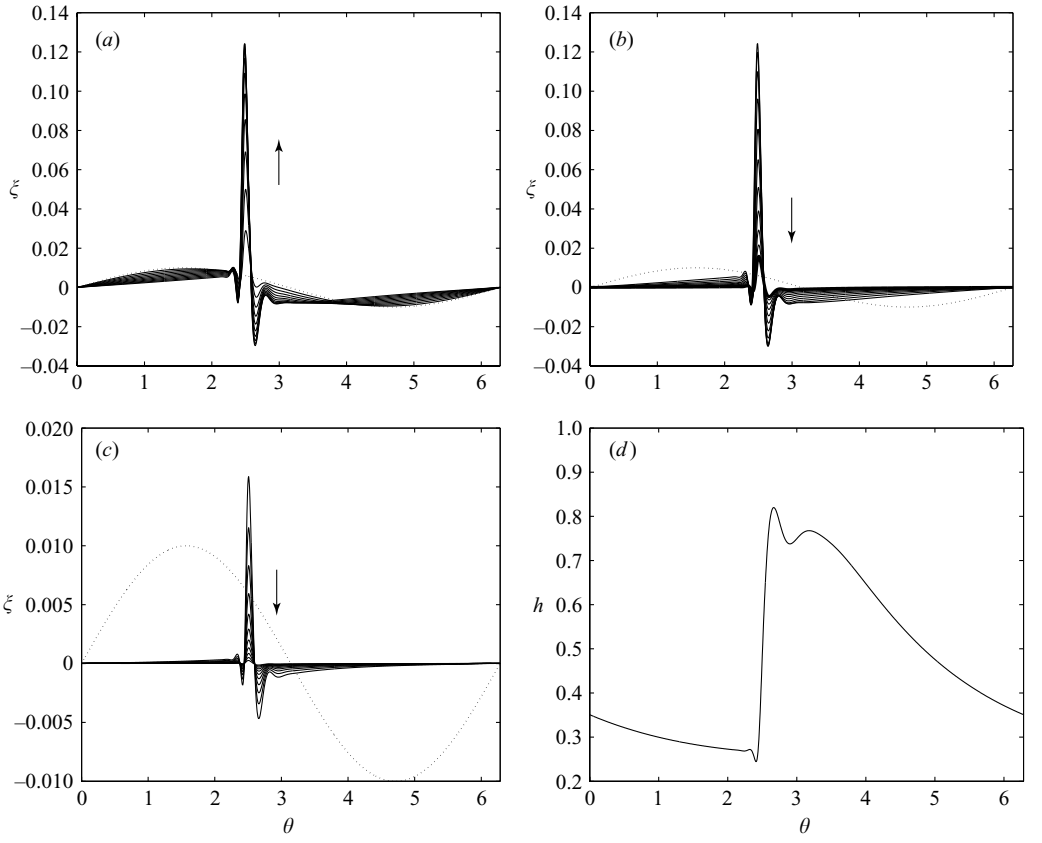

FIGURE 16. (*a*)–(*c*) The evolution of an initial perturbation, shown in (*c*), given by $\xi_0(\theta, 0) = 0.01 \sin\theta$. (*d*) The film profile corresponds to $q = 0.1825 = q_c^0$, $\gamma = -2.5$, $\delta = 0.0$, $B^{-1} = 10^{-3}$ and $\bar{h} = 0.46$.

joining the wetting profiles. In figure 18, we illustrate the essence of this process by presenting results from the full nonlinear transient code when a given rearward-facing single shock moves to a new position under the addition of positive mass through a perturbation: $\gamma = -2.5$, $\delta = 0$, $q = 0.1825$ and $B^{-1} = 10^{-5}$.

7. Conclusions

In previous studies of thin-film flow, the existence of two-dimensional ridges has been identified as a precursor to the development of axial instabilities into shark-tooth and finger patterns (Thoroddsen & Mahadevan 1997). According to classical lubrication theory, it is possible in principle to have multiple, two-dimensional, discontinuous shock profiles formed by joining positive solution branches of the flux equation. It is not currently known, however, which of these shock structures are physically realizable and consequently possible sources of the ridges. Using kinematic-wave theory, Villegas-Díaz *et al.* (2003) show that, in a lubrication model incorporating an applied surface shear, the following compressive-shock structures are stable to two-dimensional infinitesimal disturbances: single rearward-facing shocks located at any position around the cylinder when $q = q_c^0$; single forward-facing shock located on the descending side in the lower half of the cylinder when $q = q_c^\pi$; and either of these

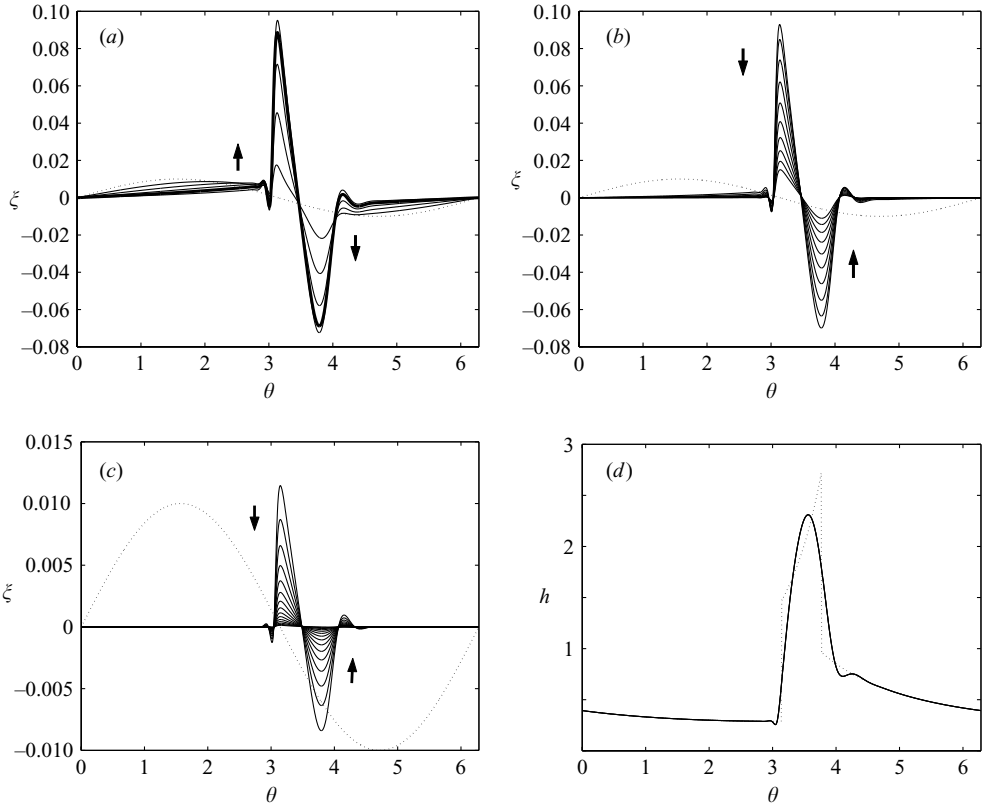

FIGURE 17. (*a*)–(*c*) The evolution of an initial perturbation, shown in (*c*), given by $\xi_0 = 0.01 \sin\theta$. (*d*) The shock profile corresponds to $q = 0.2068 = q_c^0 = q_c^\pi$, $\gamma = -2.149139$, $\delta = 0.0$, $B^{-1} = 10^{-3}$ and $\bar{h} = 0.5944$.

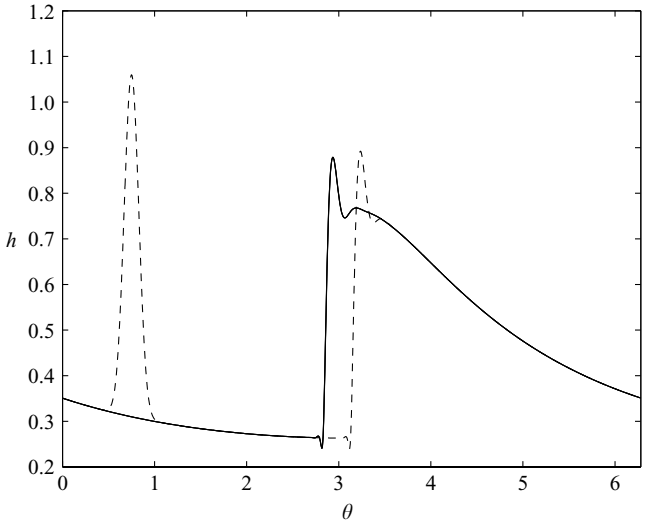

FIGURE 18. The shock is shifted towards the first quadrant by adding a perturbation of non-zero filling fraction: $q = 0.1825$, $\gamma = -2.5$, $\delta = 0.0$, $B^{-1} = 10^{-5}$. Initially $\bar{h} = 0.4151$ and finally $\bar{h} = 0.4399$.

single shocks or a double shock that comprises a rearward-facing shock located in the upper half of the cylinder and a forward-facing shock located on the descending side in the lower half of the cylinder when $q = q_c^0 = q_c^\pi$.

Although significant insight can be gained by such analysis, it is necessary to consider higher-order effects not included in the lubrication model, specifically surface-tension and gravitational smoothing, in order to gain assurance that the structures are mathematically and physically realizable. By theoretical analysis and numerical simulation, we offer support to the conjecture that the single shocks when $q = q_c^0$ or $q = q_c^\pi$ remain feasible when these higher-order smoothing effects are taken into account. These types of single shock are referred to as compressive shocks in the literature, in the sense that disturbances on each side of the shock travel toward the shock. We note that such structures are unstable to transverse perturbations, Bertozzi *et al.* (2001). On the other hand, our analysis indicates that when $q = q_c^0 = q_c^\pi$, only single rearward-facing (compressive) shocks located in the lower half of the cylinder are possible. In this case, we also found that, when the mean film thickness is larger than $\bar{h}^m$, a stable two-dimensional double structure is formed by an interaction between compressive and undercompressive shocks, where undercompressive refers to shocks through which disturbances travel. Likewise, the double-shock structure on the base profile featuring a turning point is also stable. In the case of thin-film flow down an inclined plane, this type of double-shock structure seems to be stable to transverse travelling disturbances (Bertozzi *et al.* 2001). Based on our analysis, it appears that no other type of two-dimensional shock structure is feasible, even when non-critical values of the flow rates are considered. The inclusion of an applied surface shear gives rise to the possibility of having a single stable two-dimensional shock located anywhere over the surface of the cylinder and a double shock-structure located on the descending side in the lower half of the cylinder.

Finally we note that, although unbounded solutions have been dismissed in this current study, it would be interesting to investigate the internal curtain-flow problem (see Balmer 1970), the external two-dimensional analogue of which was investigated theoretically by Wilson & Duffy (1999).

The authors would like to thank Steve Wilson for supplying a preprint of his study. M.V.D. acknowledges financial support from the Consejo de Desarrollo Cientifico y Humanistico of Universidad Central de Venezuela.

Appendix A. Governing equations

The dimensional Navier–Stokes equations for an incompressible two-dimensional flow in cylindrical coordinates (see figure 1) are

$$\frac{1}{r}\frac{\partial (ru)}{\partial r} + \frac{1}{r}\frac{\partial v}{\partial \theta} = 0, \tag{A 1}$$

$$\frac{\partial u}{\partial t} + u\frac{\partial u}{\partial r} + \frac{v}{r}\frac{\partial u}{\partial \theta} - \frac{v^2}{r} = \frac{-1}{\rho}\frac{\partial p}{\partial r} + \nu\left(\nabla^2 u - \frac{u}{r^2} - \frac{2}{r^2}\frac{\partial v}{\partial \theta}\right) - g\sin\theta, \tag{A 2}$$

$$\frac{\partial v}{\partial t} + u\frac{\partial v}{\partial r} + \frac{v}{r}\frac{\partial v}{\partial \theta} + \frac{uv}{r} = \frac{-1}{\rho r}\frac{\partial p}{\partial \theta} + \nu\left(\nabla^2 v - \frac{v}{r^2} + \frac{2}{r^2}\frac{\partial u}{\partial \theta}\right) - g\cos\theta, \tag{A 3}$$

where $\nabla^2 = \dfrac{\partial^2}{\partial r^2} + \dfrac{1}{r}\dfrac{\partial}{\partial r} + \dfrac{1}{r^2}\dfrac{\partial^2}{\partial \theta^2}$.

The velocity field $(u(r,\theta,t), v(r,\theta,t))$ and pressure field $p((r,\theta,t))$ satisfy (A 1)–(A 3) and boundary conditions (2.3)–(2.4), where

$$\boldsymbol{t} = \frac{1}{\sqrt{1+\frac{1}{r^2}\left(\frac{\partial h}{\partial\theta}\right)^2}}\left(-\frac{1}{r}\frac{\partial h}{\partial\theta}\boldsymbol{e}_r + \boldsymbol{e}_\theta\right), \quad \boldsymbol{n} = \frac{-1}{\sqrt{1+\frac{1}{r^2}\left(\frac{\partial h}{\partial\theta}\right)^2}}\left(\boldsymbol{e}_r + \frac{1}{r}\frac{\partial h}{\partial\theta}\boldsymbol{e}_\theta\right)$$

and the curvature

$$\kappa = -\left[\frac{2}{r^3}\left(\frac{\partial h}{\partial\theta}\right)^2 + \frac{1}{r} + \frac{1}{r^2}\frac{\partial^2 h}{\partial\theta^2}\right]\left[1+\left(\frac{1}{r}\frac{\partial h}{\partial\theta}\right)^2\right]^{-3/2}.$$

Using the kinematic boundary condition at the free surface $r = R - h$,

$$\frac{\mathrm{D}}{\mathrm{D}t}(r - R + h) = 0, \tag{A 4}$$

together with the continuity equation integrated radially across the film yields the flux equation

$$(R-h)\frac{\partial h}{\partial t} + \frac{\partial q}{\partial\theta} = 0, \tag{A 5}$$

where q is the azimuthal fluid flux defined by

$$q = \int_{R-h}^{R} v\,\mathrm{d}r. \tag{A 6}$$

Appendix B. Non-dimensionalization and the lubrication approximation

In the absence of surface tension, any difference between the actual flow and rigid-body rotation will, in the steady state, be caused by the draining effect of gravity. Gravitational forces scale as ρg and viscous shearing forces induced by rotation of the cylinder as $\mu\Omega R/h_0^2$; the ratio of these is $\Gamma = gh_0^2/\nu\Omega R$, which measures the relative importance of the two. Low values of Γ correspond to the case when gravity is negligible, for example in an aeroengine at extremely high rotation rates, and high values when gravity is dominant, when pooling at the bottom of the cylinder would be expected. The azimuthal velocity scale and time scale associated with rotation are ΩR and Ω^{-1}, respectively, while dynamic pressure changes are associated with the viscous pressure scale $\mu\Omega R^2/h_0^2$.

In view of the above discussion, dimensionless variables are introduced such that

$$\left.\begin{aligned} r^\star = \frac{r}{R}, \quad y^\star = \frac{R-r}{h_0}, \quad u^\star = \frac{u}{\Omega h_0}, \quad v^\star = \frac{v}{\Omega R}, \\ t^\star = \Omega t, \quad p^\star = \frac{\delta^2 p}{\mu\Omega}, \quad h^\star = \frac{h}{h_0}, \quad \kappa^\star = \frac{R\kappa}{\delta}, \end{aligned}\right\} \tag{B 1}$$

where the differing scales for u and v are forced by the continuity equation, and the free-surface curvature has been scaled on δ/R, where $\delta = h_0/R$ denotes the aspect ratio of the film, since, for films that are nearly uniform, this is the magnitude of curvature variations that generate a capillary pressure gradient.

After dropping the stars, the equations become

$$\frac{\delta u}{(1-\delta y)} - \frac{\partial u}{\partial y} + \frac{1}{(1-\delta y)}\frac{\partial v}{\partial\theta} = 0, \tag{B 2}$$

$$\delta^2\frac{\partial u}{\partial t}-\delta^2 u\frac{\partial u}{\partial y}+\frac{\delta^2 v}{r}\frac{\partial u}{\partial \theta}-\frac{\delta v^2}{r}$$
$$=\frac{1}{Re}\frac{\partial p}{\partial y}+\frac{\delta^2}{Re}\left(\frac{\partial^2 u}{\partial y^2}-\frac{\delta}{r}\frac{\partial u}{\partial y}+\frac{\delta^2}{r^2}\frac{\partial^2 u}{\partial \theta^2}-\frac{\delta^2 u}{r^2}-\frac{2\delta}{r^2}\frac{\partial v}{\partial \theta}\right)-\frac{\delta}{Fr^2}\sin\theta, \qquad (B\,3)$$

$$\frac{\partial v}{\partial t}-u\frac{\partial v}{\partial y}+\frac{v}{r}\frac{\partial v}{\partial \theta}+\frac{\delta u v}{r}$$
$$=-\frac{1}{rRe}\frac{\partial p}{\partial \theta}+\frac{1}{Re}\left(\frac{\partial^2 v}{\partial y^2}-\frac{\delta}{r}\frac{\partial v}{\partial y}+\frac{\delta^2}{r^2}\frac{\partial^2 v}{\partial \theta^2}-\frac{\delta^2 v}{r^2}+\frac{2\delta^3}{r^2}\frac{\partial u}{\partial \theta}\right)-\frac{1}{Fr^2}\cos\theta, \qquad (B\,4)$$

where Re denotes the reduced Reynolds number $\Omega R^2\delta^2/\nu$ and Fr the Froude number $\sqrt{\Omega^2 R/g}$. Most of the experimental studies have been concerned with situations where the reduced Reynolds number is small. Though some practical applications (including oil flow in aeroengines) can have large reduced Reynolds number, we restrict ourselves to the asymptotic limit $Re\to 0+$ as this may facilitate experimental verification of the theoretical results. Taking $\Gamma = Re/Fr^2 = O(1)$ and $\delta = O(1)$ as $Re\to 0+$ in the above equations reduces them to

$$-(1-\delta y)\frac{\partial u}{\partial y}+\delta u+\frac{\partial v}{\partial \theta}=0, \qquad (B\,5)$$

$$0=\frac{\partial p}{\partial y}+\delta^2\left(\frac{\partial^2 u}{\partial y^2}-\frac{\delta}{r}\frac{\partial u}{\partial y}+\frac{\delta^2}{r^2}\frac{\partial^2 u}{\partial \theta^2}-\frac{\delta^2 u}{r^2}-\frac{2\delta}{r^2}\frac{\partial v}{\partial \theta}\right)-\delta\Gamma\sin\theta, \qquad (B\,6)$$

$$0=-\frac{1}{r}\frac{\partial p}{\partial \theta}+\left(\frac{\partial^2 v}{\partial y^2}-\frac{\delta}{r}\frac{\partial v}{\partial y}+\frac{\delta^2}{r^2}\frac{\partial^2 v}{\partial \theta^2}-\frac{\delta^2 v}{r^2}+\frac{2\delta^3}{r^2}\frac{\partial u}{\partial \theta}\right)-\Gamma\cos\theta, \qquad (B\,7)$$

where $r=1-\delta y$.

The kinematic condition (A 5) at the free surface $y=h(\theta,t)$ becomes

$$(1-\delta h)\frac{\partial h}{\partial t}+\frac{\partial q}{\partial \theta}=0, \qquad (B\,8)$$

where q, non-dimensionalized using the scale $\Omega R h_0$, is defined by

$$q=\int_0^h v\,\mathrm{d}y. \qquad (B\,9)$$

The boundary condition at the cylinder surface $y=0$, (2.3), becomes

$$u=0, \qquad v=1, \qquad (B\,10)$$

while, at the free surface $y=h(\theta,t)$, the stress conditions become

$$\left(1-\left(\frac{\delta}{1-\delta h}\frac{\partial h}{\partial \theta}\right)^2\right)\left(\frac{\delta^2}{1-\delta h}\frac{\partial u}{\partial \theta}-\frac{\partial v}{\partial y}-\frac{\delta v}{1-\delta h}\right)$$
$$+\frac{2\delta^2}{1-\delta h}\frac{\partial h}{\partial \theta}\left(\frac{1}{1-\delta h}\frac{\partial v}{\partial \theta}+\frac{\delta u}{1-\delta h}+\frac{\partial u}{\partial y}\right)=-\gamma\left(1+\left(\frac{\delta}{1-\delta h}\frac{\partial h}{\partial \theta}\right)^2\right), \qquad (B\,11)$$

and

$$2\delta^2\left(-\frac{\partial u}{\partial y}+\frac{1}{1-\delta h}\frac{\partial h}{\partial \theta}\left(\frac{\delta^2}{1-\delta h}\frac{\partial u}{\partial \theta}-\frac{\partial v}{\partial y}-\frac{\delta v}{1-\delta h}\right)+\left(\frac{\delta}{1-\delta h}\frac{\partial h}{\partial \theta}\right)^2\right.$$
$$\left.\times\left(\frac{1}{1-\delta h}\frac{\partial v}{\partial \theta}+\frac{\delta u}{1-\delta h}\right)\right)\left(1+\left(\frac{\delta}{1-\delta h}\frac{\partial h}{\partial \theta}\right)^2\right)^{-1}=p-p_a-B^{-1}\kappa, \qquad (B\,12)$$

where $\gamma = T_a\delta/\mu\Omega$, $B = \Omega\mu R/\sigma\delta^3$ is the capillary number and κ is given by

$$\kappa = -\delta^{-1}\left[2\frac{\delta^2}{r^3}\left(\frac{\partial h}{\partial\theta}\right)^2 + \frac{1}{r} + \frac{\delta}{r^2}\frac{\partial^2 h}{\partial\theta^2}\right]\left[1 + \left(\frac{\delta}{r}\frac{\partial h}{\partial\theta}\right)^2\right]^{-3/2}, \tag{B 13}$$

with $r = 1 - \delta h$. The non-dimensionalization scheme used above is essentially that initially introduced by Noakes (2001). There are, of course, many other ways of proceeding. In order to remove Γ from the problem, Benjamin *et al.* (1993) and Villegas-Díaz *et al.* (2003) take the film scale $h_0 = (\nu\Omega R/g)^{1/2}$; Benjamin *et al.* thus use a hydrostatic scale for the pressure and the aspect ratio and dimensionless applied stress become, respectively,

$$\delta = \frac{h_0}{R} = \sqrt{\frac{\Omega\nu}{gR}}, \quad \gamma = \frac{T_a}{\sqrt{\rho g\mu\Omega R}}. \tag{B 14}$$

Hosoi & Mahadevan (1999) use this same non-dimensionalization except that they focus on inertial instabilities and use the slow time scale R^2/ν, rather than the fast one Ω^{-1}. Ashmore *et al.* (2003) use an approach very close to the current one except that they use the filling fraction, rather than the aspect ratio, as a more naturally defined small parameter.

Appendix C. Asymptotic development of the governing equations

Equations (B 5)–(B 7), subject to the boundary conditions (B 10), (B 11) and (B 12), determine the dynamics of the flow. In order to make further analytical progress we now exploit the fact that the aspect ratio δ is very small in many practical situations. It is natural therefore to seek asymptotic expansions in the form

$$(u, v, p) = (u_0, v_0, p_0) + \delta(u_1, v_1, p_1) + \delta^2(u_2, v_2, p_2) + O(\delta^3). \tag{C 1}$$

C.1. *Leading-order solution*

Without loss of generality, the constant $O(\delta^{-1})$-term from the curvature can be absorbed into the constant p_a. We keep the surface-tension effect at the leading order, even though in most practical situations the magnitude of the inverse capillary number is very small, since at a shock front the magnitude of the high-order derivatives of the film thickness can be very large.

The leading-order system is straightforward to obtain and solve; the key results are

$$p_0 = p_a - B^{-1}\left(h + \frac{\partial^2 h}{\partial\theta^2}\right), \tag{C 2}$$

$$v_0 = 1 + \gamma y + \left(\Gamma\cos\theta - B^{-1}\frac{\partial}{\partial\theta}\left(h + \frac{\partial^2 h}{\partial\theta^2}\right)\right)\left(\tfrac{1}{2}y^2 - hy\right). \tag{C 3}$$

C.2. *First-order solution*

Similarly, the key results here are

$$p_1 = (y - h)\Gamma\sin\theta - B^{-1}\left(h^2 + 2h\frac{\partial^2 h}{\partial\theta^2} + \tfrac{1}{2}\left(\frac{\partial h}{\partial\theta}\right)^2\right), \tag{C 4}$$

$$v_1 = -y + \gamma\left(\tfrac{1}{2}y^2 - 2hy\right) + \Gamma\cos\theta\left(\tfrac{3}{2}h^2y - hy^2 + \tfrac{1}{3}y^3\right)$$
$$+ \Gamma\sin\theta\frac{\partial h}{\partial\theta}\left(hy - \tfrac{1}{2}y^2\right) + B^{-1}\frac{\partial}{\partial\theta}\left(h + \frac{\partial^2 h}{\partial\theta^2}\right)\left(-\tfrac{1}{2}h^2y + \tfrac{1}{2}hy^2 - \tfrac{1}{3}y^3\right)$$
$$+ B^{-1}\frac{\partial}{\partial\theta}\left(h^2 + 2h\frac{\partial^2 h}{\partial\theta^2} + \tfrac{1}{2}\left(\frac{\partial h}{\partial\theta}\right)^2\right)\left(hy - \tfrac{1}{2}y^2\right). \quad \text{(C 5)}$$

Thus, to $O(\delta)$, the profile evolves according to

$$(1 - \delta h)\frac{\partial h}{\partial t} + \frac{\partial q}{\partial\theta} = 0, \quad \text{(C 6)}$$

where

$$q = \int_0^h (v_0 + \delta v_1)\,\mathrm{d}y$$
$$= h + \tfrac{1}{2}\gamma h^2 - \tfrac{1}{3}h^3\left(\Gamma\cos\theta - B^{-1}\frac{\partial}{\partial\theta}\left(h + \frac{\partial^2 h}{\partial\theta^2}\right)\right)$$
$$+ \delta\left[-\tfrac{1}{2}h^2 - \tfrac{5}{6}\gamma h^3 + \tfrac{1}{2}\Gamma h^4\cos\theta + \tfrac{1}{3}\Gamma h^3\frac{\partial h}{\partial\theta}\sin\theta\right.$$
$$\left. - \tfrac{1}{6}h^4B^{-1}\frac{\partial}{\partial\theta}\left(h + \frac{\partial^2 h}{\partial\theta^2}\right) + \tfrac{1}{3}h^3B^{-1}\frac{\partial}{\partial\theta}\left(h^2 + 2h\frac{\partial^2 h}{\partial\theta^2} + \tfrac{1}{2}\left(\frac{\partial h}{\partial\theta}\right)^2\right)\right]. \quad \text{(C 7)}$$

Neglecting surface tension corresponds to the classical lubrication limit; the system (C 6), (C 7) with $\delta = B^{-1} = 0$ is termed the 'lubrication model'.

REFERENCES

Ashmore, J. J., Hosoi, A. H. & Stone, H. A. 2003 The effect of surface tension on rimming flows in a partially filled rotating cylinder. *J. Fluid Mech.* **479**, 65–98.

Balmer, R. T. 1970 The hygrocyst, a stability phenomenon in continuum mechanics. *Nature* **227**, 600–601.

Benilov, E. S., O'Brien, S. B. G. & Sazonov, I. A. 2003 A new type of instability: explosive disturbances in a liquid film inside a rotating horizontal cylinder. *J. Fluid Mech.* **497**, 201–224.

Benjamin, T. B., Pritchard, W. G. & Tavener, S. J. 1993 Steady and unsteady flows of a highly viscous liquid inside a rotating horizontal cylinder. Preprint.

Bertozzi, A. L., Munch, A. & Shearer, M. 1999 Undercompressive waves in driven film flow: theory, computation, and experiment. *Stud. Adv. Maths* **13**, 43–67.

Bertozzi, A. L., Munch, A., Shearer, M. & Zumbrun, K. 2001 Stability of compressive and undercompressive thin film travelling waves. *Eur. J. Appl. Maths* **12**, 253–291.

Black, G. J. B. 2002 Theoretical studies of thin-film flows. MSc thesis, University of Strathclyde.

Hosoi, A. E. & Mahadevan, L. 1999 Axial instability of a free surface front in a partially filled horizontal rotating cylinder. *Phys. Fluids* **11**, 97–106.

Johnson, R. E. 1988 Steady-state coating flows inside a rotating horizontal cylinder. *J. Fluid Mech.* **190**, 321–342.

Johnson, R. E. 1990 In *Engineering Science, Fluid Dynamics: A Symposium to Honor T. Y. Wu.* World Scientific, Singapore.

Moffatt, H. K. 1977 Behaviour of a viscous film on the outer surface of a rotating cylinder. *J. Méc.* **16**, 651–673.

Noakes, C. J. 2001 The dynamics of liquid films on rotating surfaces. PhD thesis, University of Nottingham.

Noakes, C. J., King, J. R. & Riley, D. S. 2005 On three-dimensional stability of a uniform, rigidly rotating film on a rotating cylinder. *Q. J. Mech. Appl. Maths* **58**, 229–256.

O'Brien, S. B. G. 2002*a* Linear stability of rimming flow. *Q. Appl. Maths* **40**, 201–211.

O'Brien, S. B. G. 2002*b* A mechanism for linear instability in two-dimensional rimming flow. *Q. Appl. Maths* **40**, 283–299.

O'Brien, S. B. G. & Gath, E. G. 1998 The location of a shock in a rimming flow. *Phys. Fluids* **10**, 1040–1042.

Orr, F. M. & Scriven, L. E. 1978 Rimming flow: numerical simulation of steady, viscous, free-surface flow with surface tension. *J. Fluid Mech.* **84**, 145–165.

Revallo, M. & Riley, D. S. 2004 On two-dimensional rapidly rotating rimming flow subject to gravitational perturbation and a constant surface shear. Preprint.

Ruschak, K. J. & Scriven, L. E. 1976 Rimming flow of liquid in a rotating horizontal cylinder. *J. Fluid Mech.* **76**, 113–125.

Thoroddsen, S. T. & Mahadevan, L. 1997 Experimental study of coating flows in a partially-filled horizontally rotating cylinder. *Exps. Fluids* **23**, 1–13.

Tirumkudulu, M. & Acrivos, A. 2001 Coating flows within a rotating horizontal cylinder: lubrication analysis, numerical computations, and experimental measurements. *Phys. Fluids* **13**, 14–19.

Villegas-Díaz, M., Power, H. & Riley, D. S. 2003 On the stability of rimming flows to two-dimensional disturbances. *Fluid Dyn. Res.* **33**, 141–172.

Wilson, S. D. R. & Williams, J. 1997 The flow of a liquid film on the inside of a rotating cylinder, and some related problems. *Phys. Fluids* **9**, 2184–2190.

Wilson, S. K. & Duffy, B. R. 1999 Thin-film and curtain flows on the outside of a rotating horizontal cylinder. *J. Fluid Mech.* **394**, 29–49.

Wilson, S. K., Duffy, B. R. & Black, G. J. B. 2004 Thin-film flow on a stationary or uniformly rotating horizontal cylinder subject to a prescribed uniform shear stress at the free surface of the film. Preprint.

Wilson, S. K., Hunt, R. & Duffy, B. R. 2002 On the critical solutions in coating and rimming flow on a uniformly rotating horizontal cylinder. *Q. J. Mech. Appl. Maths* **55**, 357–387.